

EM41/Diris W. 167P

Final

11-93-11

2011

60676

"BATSE Data Analysis"

FINAL REPORT

Contract NAS8-38609
Delivery Order Number 100

February 16, 1994 - May 15, 1995

Prepared by

Dr. William S. Paciesas

Prepared for
George C. Marshall Space Flight Center
National Aeronautics and Space Administration
Marshall Space Flight Center, Alabama 35812

Submitted by
Department of Physics
The University of Alabama in Huntsville
Huntsville, Alabama 35899

June 1995

1. INTRODUCTION

The Burst and Transient Source Experiment (BATSE) is one of four instruments on the Compton Observatory which was launched by the space shuttle Atlantis on April 5, 1991. As of mid-May, 1995, BATSE detected more than 1,280 cosmic gamma-ray bursts and more than 750 solar flares. Pulsed gamma-rays have been detected from at least 17 sources and emission from at least 31 sources (including most of the pulsed sources) has been detected by the Earth occultation technique. UAH participation in BATSE is extensive but can be divided into two main areas, operations and data analysis. The daily BATSE operations tasks represent a substantial level of effort and involve a large team composed of MSFC personnel as well as contractors such as UAH. The scientific data reduction and analysis of BATSE data is also a substantial level of effort in which UAH personnel have made significant contributions.

2. MISSION OPERATIONS

W. Paciesas served as BATSE Mission Operations Software (MOPS) Development Manager, chairing the Level V Configuration Control Board for the MOPS software. Paciesas also supervised distribution of the Individual Burst Data Base (IBDB) files to co-investigators at Goddard Space Flight Center (GSFC) and the University of California, San Diego (UCSD), and to the CGRO Science Support Center. K. Squier produced software to convert the MOPS burst catalog into the new format, now called the MOPS trigger catalog, and to populate certain fields in the new catalog using data read directly from the archived daily datasets. Squier also enhanced the capabilities of IBDB_REPORT to display additional IBDB data contents. V. Chaganti incorporated various improvements to the HER/SHER correction software, including correction of the first HERB/SHERB readout records and merging these with the corrected HER/SHER files. K. Deal, Z. Shariff, T. Koshut, R. Mallozzi and G. Richardson assisted in daily data and burst operations as required.

3. BURST DATA ANALYSIS

The second BATSE burst catalog was completed and put on-line at CGROSSC in June 1994. Koshut, Shariff, Chaganti, Mallozzi and G. Pendleton all contributed essential work on the basic catalog

analysis. Pendleton produced response matrices which were used for catalog flux/fluence measurements and burst locations, and are of general use for spectral analysis¹. M. Briggs conducted basic studies of burst angular distribution statistics for the second catalog². J. Brainerd was heavily involved in searches for evidence of repetition in the burst sky distribution. In collaboration with C. Meegan (MSFC) and others, he derived upper limits to the fraction of repeaters using nearest neighbor and two-point correlation analyses, and also derived upper limits to temporal/spatial burst clustering using a Monte Carlo technique^{3,4}.

Paciesas continued to manage the burst spectral analysis effort. Results from the burst spectroscopy team's visual search for spectral lines were published⁵⁻⁹. Detailed plans for an exhaustive automated search for spectral features were formulated at a meeting of the burst spectroscopy team in San Diego on 17-18 Feb 1994. M. Briggs is leading the exhaustive search effort.

Burst spectroscopy team results on continuum spectral analysis were also published^{10,11}. Preece investigated low-energy components using the DISCSP channel 1 of the BATSE spectroscopy detectors¹² and also continued collaborative studies of burst high-energy spectra¹³. Preece & Pendleton continued their work on systematic studies of burst spectra for eventual inclusion in a burst spectroscopy catalog^{14,15}. Brainerd studied BATSE data on GRB durations and showed that effects which mimic cosmological time dilation may be expected from an ensemble of bursts that is spatially limited in Euclidean space¹⁶.

Graduate students Koshut and Mallozzi continued work on burst data analysis as part of their Ph.D. dissertations. Koshut studied characteristics of GRB precursors as compared with those of the main GRB emission¹⁷. Mallozzi tested GRB spectra for consistency with cosmological models by measuring the peak energy of burst νF_ν spectra as a function of burst peak intensity¹⁸.

Paciesas continued to participate in collaborative studies of burst temporal characteristics^{19,20}. Pendleton, Briggs, Paciesas and Mallozzi were involved in collaborative studies of model constraints derived from the burst luminosity distribution²¹⁻²³. Mallozzi and Koshut collaborated with J. Horack (MSFC) and others on a study of constraints on heliospheric GRB models derived from BATSE data²⁴. Briggs and

Pendleton collaborated with D. Hartmann (Clemson) & others on tests of galactic GRB models using BATSE data²⁵.

4. NON-BURST DATA ANALYSIS

Paciesas worked with N. Zhang (USRA), A. Harmon (MSFC) & others to develop algorithms for producing images derived from occultation analysis & to study systematic effects in occultation imaging²⁶⁻²⁸. Paciesas continued studies of long-term variability of Cygnus X-1 and participated in collaborative studies of the X-ray nova GRO J1655-40²⁹ discovered by BATSE and now known to be a superluminal radio jet source. Graduate student K. Deal completed an M.S. thesis on the long-term occultation observations of GRS 1915+105, the other known superluminal radio jet source in the Galaxy³⁰. Paciesas & Deal, with Harmon, Zhang & others, studied hard x-ray/radio correlations in the two superluminal jet sources^{31,32}.

Paciesas continued collaborative efforts involving multi-wavelength studies of GRO J0422+32³³ and 3C 273³⁴. Graduate student M. Stollberg continued studies of the X-ray pulsar EXO 2030+375 as part of his Ph.D. dissertation. Pendleton collaborated in studies of the newly discovered X-ray pulsar GRO J1948+32³⁵.

5. PRESENTATIONS AND OTHER ACTIVITIES

Brainerd completed co-editing of the proceedings of the Second Huntsville Gamma-Ray Burst Workshop³⁶. Paciesas attended the IAU Symposium on Compact Stars in Binaries, The Hague, The Netherlands (15-19 Aug 1994), presenting a poster on studies of the long-term variability of Cygnus X-1 and a talk on the newly discovered X-ray transient GRO J1655-40²⁹. Brainerd attended the summer workshop on gamma-ray bursts in Aspen, CO (29 Aug-11 Sep 1994). Paciesas attended the workshop on Imaging in High-Energy Astronomy (Anacapri, Italy, 26-30 Sep 1994), presenting a talk on the effects of background subtraction on occultation imaging²⁸. Koshut, Paciesas, Pendleton & Preece attended the AAS/HEAD meeting (Napa, CA, 2-5 Nov 1994). Paciesas presented a poster on Cyg X-1 long-term variability and gave a short talk on BATSE observations of GRS 1915+105; Pendleton discussed burst continuum spectral properties; Preece discussed high-energy spectral evolution of bursts; Koshut presented results of his study of burst precursors.

Paciesas attended the IAU Colloquium on Flares & Flashes in Sonneberg, Germany (5-9 Dec 1994) and the 17th Texas Symposium on Relativistic Astrophysics in Munich, Germany (12-17 Dec 1994). In the former meeting he presented an invited review talk on BATSE as a hard X-ray all-sky monitor. In the latter meeting he presented a contributed paper on BATSE observations of GRS 1915+105 and GRO J1655-40³¹. Brainerd and Briggs also attended the Texas Symposium, where Briggs presented an invited review talk on BATSE observations of the spectra of gamma-ray bursts³⁷. Following this, they traveled to Moscow, Russia, for discussions with I. Mitrofanov (IKI) and other collaborators on studies of the average intensity and spectral evolution of BATSE GRBs.

Deal, Paciasas & Stollberg attended the AAS meeting in Tucson, AZ (8-12 Jan 1995). Deal & Stollberg presented posters on BATSE observations of GRS 1915+105 and EXO 2030+375, respectively. Paciasas participated in a press conference with C. Wilson (MSFC) and R. Hjellming (NRAO), discussing the galactic superluminal radio jet source GRO J1655-40. Briggs attended the workshop on High-velocity Neutron Stars and Gamma-Ray Bursts in San Diego, CA (15-17 Mar 1995), presenting a talk on galactic neutron star model constraints derived from BATSE data². Briggs & Preece attended the ESLAB Symposium "Towards the Source of Gamma-Ray Bursts in Noordwijk, the Netherlands (25-29 Apr 1995). Briggs presented an invited review of BATSE burst observations³⁸. Preece presented papers on time-resolved burst spectroscopy¹⁴ and studies of burst spectra at low energies¹².

REFERENCES

- [1] "The detector response matrices of the burst and transient source experiment (BATSE) on the Compton Gamma Ray Observatory," **G.N. Pendleton, W.S. Paciesas, R.S. Mallozzi, T.M. Koshut, G.J. Fishman, C.A. Meegan, R.B. Wilson, J.M. Horack & J.P. Lestrade**, *Nucl. Inst. Meth.*, submitted (1995).
- [2] "GRB Moments: HVNS Models Compared with BATSE Observations," **M.S. Briggs, G.N. Pendleton, W.S. Paciesas, J. Hakkila, D. Hartmann, C. Kouveliotou, C.A. Meegan & G.J. Fishman**, in *Proc. UCSD Workshop on High-Velocity Neutron Stars & Gamma-Ray Bursts*, in press (1995).
- [3] "Time-Dependent Clustering Analysis of the Second BATSE Gamma-Ray Burst Catalog," **J.J. Brainerd, C.A. Meegan, M.S. Briggs, G.N. Pendleton & M.N. Brock**, *Ap. J.*, **L39** (1995).
[see attachment]
- [4] "Do Gamma-Ray Burst Sources Repeat?" **C.A. Meegan, D.H. Hartmann, J.J. Brainerd, M. Briggs, W.S. Paciesas, G. Pendleton, C. Kouveliotou, G. Fishman, G. Blumenthal & M. Brock**, *Ap. J.* **446**, L15 (1995).
- [5] "BATSE Gamma-Ray Burst Line Search: I. Search for Narrow Lines in Spectroscopy Detector Data," **D.M. Palmer, B.J. Teegarden, B.E. Schaefer, T.L. Cline, D.L. Band, L.A. Ford, J.L. Matteson, W.S. Paciesas, G.N. Pendleton, M.S. Briggs, R.D. Preece, G.J. Fishman, C.A. Meegan, R.B. Wilson & J.P. Lestrade**, *Ap. J.*, **433**, L77 (1994).
- [6] "BATSE Gamma-Ray Burst Line Search: II. Bayesian Consistency Methodology," **D.L. Band, L.A. Ford, J.L. Matteson, M. Briggs, W. Paciesas, G. Pendleton, R. Preece, D. Palmer, B. Teegarden & B. Schaefer**, *Ap. J.*, **434**, 560 (1994).
- [7] "BATSE Gamma-Ray Burst Line Search: III. Line Detectability," **D.L. Band, L.A. Ford, J.L. Matteson, M.S. Briggs, W.S. Paciesas, G.N. Pendleton, R.D. Preece, D.M. Palmer, B.J. Teegarden & B.E. Schaefer**, *Ap. J.*, **447**, 289 (1995).
- [8] "The BATSE Search for Absorption Lines," **D.L. Band, L.A. Ford, J.L. Matteson, D.M. Palmer, B.J. Teegarden, M.S. Briggs, G.N. Pendleton, R.D. Preece & W.S. Paciesas**, in *Proc. UCSD Workshop on High-Velocity Neutron Stars & Gamma-Ray Bursts*, in press (1995).
- [9] "The Evaluation of BATSE Line Candidates," **D. L. Band, S. Ryder, L. A. Ford, J. L. Matteson, D. M. Palmer, B. J. Teegarden, M. S. Briggs, W. S. Paciesas, G. N. Pendleton and R. D. Preece**, *Astrophys. Sp. Sci.*, in press (1995).

- [10] "Spectral Evolution of a Subclass of Gamma Ray Bursts Observed by BATSE," P.N. Bhat, G.J. Fishman, C.A. Meegan, R.B. Wilson, C. Kouveliotou, **W.S. Paciesas**, **G.N. Pendleton** and B.E. Schaefer, *Ap. J.*, **426**, 604 (1994).
- [11] "BATSE Observations of Gamma-Ray Burst Spectra: II. Peak Energy Evolution in Bright, Long Bursts," L.A. Ford, D.L. Band, J.L. Matteson, **M.S. Briggs**, **G.N. Pendleton**, **R.D. Preece**, **W.S. Paciesas**, B.J. Teegarden, D.M. Palmer, B.E. Schaefer, T.L. Cline, G.J. Fishman, C. Kouveliotou, C.A. Meegan, R.B. Wilson & J.P. Lestrade, *Ap. J.*, in press (1995).
- [12] "GRBs in the 5-10 keV Regime as Seen by BATSE," **R.D. Preece**, **M.S. Briggs**, **G.N. Pendleton**, **W.S. Paciesas**, D.L. Band & L.A. Ford, *Astrophys. Sp. Sci.*, in press (1995).
- [13] "Spectral Characterisation of Gamma-Ray Bursts with COMPTEL and BATSE," L.O. Hanlon, K. Bennett, O.R. Williams, C. Winkler & **R.D. Preece**, *Astrophys. Sp. Sci.*, in press (1995).
- [14] "BATSE Time-Resolved Observations of GRBs: The Burst 'Topographic' Map," **R.D. Preece**, **M.S. Briggs**, **G.N. Pendleton**, **W.S. Paciesas**, D.L. Band & L.A. Ford, *Astrophys. Sp. Sci.*, in press (1995).
- [15] "The Continuum Spectral Characteristics of Gamma-Ray Bursts Observed by BATSE," **G.N. Pendleton**, **W.S. Paciesas**, **M.S. Briggs**, **R.S. Mallozzi**, **T.M. Koshut**, G.J. Fishman, C.A. Meegan, R.B. Wilson, B.A. Harmon & C. Kouveliotou, *Ap. J.*, **431**, 416 (1994). [see attachment]
- [16] "Mimicking within Euclidean Space a Cosmological Time Dilation of Gamma-Ray Burst Durations," J.J. Brainerd, *Ap. J.*, **428**, L1 (1994). [see attachment]
- [17] "Gamma-Ray Burst Precursor Activity as Observed with BATSE," **T.M. Koshut**, C. Kouveliotou, **W.S. Paciesas**, J. van Paradijs, **G.N. Pendleton**, **M.S. Briggs**, G.J. Fishman & C.A. Meegan, *Ap. J.*, in press (1995).
- [18] "The vF_v Peak Energy Distributions of Gamma-Ray Bursts Observed by BATSE," **R.S. Mallozzi**, **W.S. Paciesas**, **G.N. Pendleton**, **M.S. Briggs**, **R.D. Preece**, C.A. Meegan and G.J. Fishman, *Ap. J.*, in press (1995).
- [19] "Gross Spectral Differences between Bright and Dim Gamma-Ray Bursts," R.J. Nemiroff, J.P. Norris, J.T. Bonnell, W.A.D.T. Wickramasinghe, C. Kouveliotou, **W.S. Paciesas**, G.J. Fishman & C. A. Meegan, *Ap. J.*, **435**, L133 (1994).
- [20] "Duration Distributions of Bright and Dim BATSE Gamma-Ray Bursts," J.P. Norris, J.T. Bonnell, R.J. Nemiroff, J.D. Scargle, C. Kouveliotou, **W.S. Paciesas**, C.A. Meegan & G.J. Fishman, *Ap. J.*, **439**, 542 (1995).

- [21] "Constraints on the Luminosities of Gamma-Ray Bursts," J. Hakkila, C. Meegan, J. Horack, **G. Pendleton**, **M. Briggs**, **W. Paciesas**, G. Emslie & R. Mallozzi, *Astrophys. Sp. Sci.*, in press (1995).
- [22] "Constraints on the Luminosities of Galactic Gamma-Ray Bursts," J. Hakkila, C. A. Meegan, J. M. Horack, **G. N. Pendleton**, **M. S. Briggs**, **W. S. Paciesas** and A. G. Emslie, in *Proc. UCSD Workshop on High-Velocity Neutron Stars & Gamma-Ray Bursts*, in press (1995).
- [23] "Galactic Gamma-Ray Burst Models: Constraints on the Intrinsic Luminosity Function," J. Hakkila, C.A. Meegan, **G.N. Pendleton**, J.M. Horack, **M.S. Briggs**, **W.S. Paciesas** & A.G. Emslie, *Ap. J.*, in press (1995).
- [24] "Implications of the BATSE Data for a Heliocentric Origin of Gamma-Ray Bursts," J.M. Horack, **T.M. Koshut**, **R.S. Mallozzi**, S.D. Storey & A.G. Emslie, *Ap. J.*, **429**, 319 (1994).
- [25] "Are Galactic GRB Models Still an Option?" D.H. Hartmann, **M.S. Briggs**, **G.N. Pendleton** & J.Hakkila, *Astrophys. Sp. Sci.*, in press (1995).
- [26] "A Maskless Gamma-Ray All-Sky Imager: BATSE/CGRO," S.N. Zhang, G.J. Fishman, B.A. Harmon, **W.S. Paciesas**, C.A. Meegan, R.B. Wilson, M.H. Finger & B.C. Rubin, *IEEE Trans. Nucl. Sci.*, **41**, 1313 (1994).
- [27] "Hard X-Ray All-Sky Imaging with BATSE/CGRO," S.N. Zhang, B.A. Harmon, G.J. Fishman & **W.S. Paciesas**, *Experimental Astronomy*, in press (1995).
- [28] "A Study of the Effects of Background Subtraction on Occultation Imaging," **W.S. Paciesas**, S.N. Zhang, B.C. Rubin, B.A. Harmon & G.J. Fishman, to be published in *Imaging in High Energy Astronomy*, ed. L. Bassani and G. di Cocco (1995). [see attachment]
- [29] "Discovery of a New X-Ray Transient in Scorpius," **W.S. Paciesas**, S.N. Zhang, B.C. Rubin, B.A. Harmon, C.A. Wilson & G.J. Fishman, to be published in *Compact Stars in Binaries*, ed. J. van Paradijs, E. Kuulkers & E.P.J. van den Heuvel (1996). [see attachment]
- [30] "BATSE Observations of the X-Ray Transient GRS 1915+105," **K.J. Deal**, M.S. thesis, University of Alabama in Huntsville (1995).
- [31] "BATSE Observations of GRS 1915+105 and GRO J1655-40," **W.S. Paciesas**, **K.J. Deal**, B.A. Harmon, C.A. Wilson, S.N. Zhang & G.J. Fishman, *Ann. NY Acad. Sci.*, in press (1995). [see attachment]
- [32] "Correlations between X-ray outbursts and relativistic ejections in the X-ray transient GRO J1655-40," B.A. Harmon, C.A. Wilson, S.N. Zhang, **W.S. Paciesas**, G.J. Fishman, R.M.

Hjellming, M.P. Rupen, D.M. Scott, M.S. Briggs & B.C. Rubin, *Nature* **374**, 703 (1995).

- [33] "Observations of the X-Ray Transient GRO J0422+32: I. Outburst and the Decay to Quiescence," P.J. Callanan, M.R. Garcia, J.E. McClintock, P. Zhao, R.R. Remillard, C.D. Bailyn, J.A. Orosz, B.A. Harmon & W.S. Paciesas, *Ap. J.*, **441**, 786 (1995).
- [34] "Simultaneous and quasi-simultaneous observations of the continuum emission of the quasar 3C 273 from radio to gamma-ray energies," G.G. Lichti, T. Balonek, T.J.-L. Courvoisier, N. Johnson, M. McConnell, B. McNamara, C. von Montigny, W. Paciesas, E.I. Robson, A. Sadun, C. Schalinski, A.G. Smith, R. Staubert, H. Steppe, B.N. Swanenburg, M.J.L. Turner, M.-H. Ulrich & O.R. Williams, *Astr. Ap.*, in press (1995).
- [35] "Discovery of the 18.7 Second Accreting X-Ray Pulsar GRO J1948+32," D. Chakrabarty, T. Koh, L. Bildsten, T.A. Prince, M.H. Finger, R. B. Wilson, G.N. Pendleton & B.C. Rubin, *Ap.J.*, in press (1995).
- [36] *Gamma-Ray Bursts: Second Workshop, Huntsville, AL 1993*, ed. G.J. Fishman, J.J. Brainerd & K. Hurley (New York: AIP) (1994).
- [37] "BATSE Observations of the Spectra of Gamma-Ray Bursts," M.S. Briggs, *Ann. NY Acad. Sci.*, in press (1995).
- [38] "Four Years of BATSE Gamma-Ray Burst Observations," M.S. Briggs, *Astrophys. Sp. Sci.*, in press (1995).

ATTACHMENTS

TIME-DEPENDENT CLUSTERING ANALYSIS OF THE SECOND BATSE GAMMA-RAY BURST CATALOG

J. J. BRAINERD,^{1,2} C. A. MEEGAN,³ MICHAEL S. BRIGGS,¹ G. N. PENDLETON,¹ AND M. N. BROCK³

Received 1994 August 11; accepted 1994 December 14

ABSTRACT

A time-dependent two-point correlation-function analysis of the BATSE 2B catalog finds no evidence of burst repetition. As part of this analysis, we discuss the effects of sky exposure on the observability of burst repetition and present the equation describing the signature of burst repetition in the data. For a model of all burst repetition from a source occurring in less than five days we derive upper limits on the number of bursts in the catalog from repeaters and model-dependent upper limits on the fraction of burst sources that produce multiple outbursts.

Subject heading: gamma rays: bursts

1. INTRODUCTION

Gamma-ray burst observations by the Burst and Transient Source Experiment (BATSE) on the *Compton Gamma-Ray Observatory* (CGRO) have tightened the geometric constraints on galactic gamma-ray burst models to the point that an extragalactic origin now provides the most natural explanation for the gamma-ray burst spatial distribution (Briggs et al. 1995; Hakkila et al. 1994). The question that now must be answered is what useful constraints can be placed on models of extragalactic gamma-ray bursts by the observations. One of the more important constraints is on the rate at which sources produce gamma-ray bursts. If burst repetition were proven, then destructive burst models such as the merging neutron star model would be disproven and other models would have limits placed on their energy production mechanisms.

If gamma-ray burst sources repeat, one expects them to produce small-scale clustering, with the clustering scale set by the burst location error. Several authors have analyzed with mixed results the 1B Gamma-Ray Burst Catalog for small-scale clustering (Blumenthal et al. 1994; Quashnock & Lamb 1993). A subsequent analysis of the 2B catalog finds no evidence of burst clustering or repetition with either a two-point correlation-function analysis or a nearest neighbor analysis and places an upper limit of $\sim 20\%$ on the fraction of bursts observed as repeater bursts (Meegan et al. 1995).

Wang and Lingenfelter have conducted a time-dependent analysis of the 1B catalog (Wang & Lingenfelter 1993, 1994). The first article argues that five bursts with overlapping location errors are from a single source. The second article presents the results of a time dependent two-point correlation-function analysis of the 1B catalog. They find an excess of burst pairs with separations of $t < 5$ days and $\theta < 4^\circ$ which they assert is statistically significant and evidence of burst repetition.

In this *Letter* we perform a time-dependent two-point correlation-function analysis of the 2B catalog (Meegan et al. 1994) on both the full catalog of 585 bursts and the subset of 485 bursts with non-MAXBC locations (defined in § 2). In § 2 we discuss the effect of Earth blockage, trigger off-time, and data loss on the ability of BATSE to observed burst repetition. The polynomial time variable τ defined by Wang & Lingenfel-

ter and the effects of a variable burst detection rate are discussed in § 3. We discuss the expected behavior of the two-point correlation-function in § 4, and we give our results from such an analysis of the 2B catalog in § 5.

2. DETECTING REPEATING BURSTS

The number of bursts that BATSE can detect from a repeating source is dependent on the fraction of the sky occulted by Earth and the fraction of time the burst trigger is enabled. These effects are easily modeled if one assumes that the interval of time between outbursts is long compared to the orbital period of the spacecraft, so that the probability of observing each outburst from a source is uncorrelated with the observation of previous outbursts. Generally a repeater must produce many bursts above threshold for BATSE to observe two or more bursts from the same source. A consequence of this is that the observations set stronger constraints on the repetition models with high intrinsic burst rates than those with low intrinsic burst rates.

Because the CGRO tape recorders failed in the second year of operation, a significant fraction of bursts in the 2B catalog only have locations determined from the MAXBC data type—the maximum count rate over 1 s in each detector module in the 50 keV to 300 keV energy band. In contrast, all bursts in the 1B catalog have non-MAXBC locations. The MAXBC data type is the most problematic BATSE data type for locations, producing locations with larger errors than the other BATSE data types. Exclusion of MAXBC positions from a sample improves the overall location error at the expense of a smaller trigger enable time. Meegan et al. (1994) find that the signal of repetition in the two-point correlation-function is proportional to the sky exposure regardless of the underlying repetition model. Therefore, if MAXBC locations are excluded, a signal for burst repetition would be $\approx 25\%$ smaller in the 2B catalog than in the 1B catalog. This loss is almost precisely compensated for by the better statistics from the larger sample size.

3. DISTRIBUTION OF BURST TIME SEPARATIONS

If bursts were detected at a uniform rate over a time interval T , the time separation Δt of pairs of bursts would be uniformly distributed in the variable

$$\tau = 1 - \left(1 - \frac{\Delta t}{T}\right)^2 \quad (1)$$

¹ University of Alabama in Huntsville.

² Space Sciences Laboratory, ES-84, NASA Marshall Space Flight Center, Huntsville, AL 35812; brainerd@ssl.mfsc.nasa.gov

³ NASA Marshall Space Flight Center.

(Wang & Lingenfelter 1994). For N bursts, the average number of burst pairs per unit τ is $N(N-1)/2$ if the instrument is always on and if the burst trigger threshold is constant; as discussed below, both of these assumptions are false, but for the present discussion we accept them as true.

A uniform distribution of burst pairs with τ does not imply a normal distribution in τ . In fact, the distribution of burst pairs in τ is highly correlated, and this correlation is different for different intervals in τ . For instance, if the interval $0 < \tau < 1$ is divided into n subintervals of equal size, then the number of burst pairs in the subinterval $0 < \tau < 1/n$ for a particular burst decreases by one and increases by an arbitrary amount over the number of pairs in this interval for the preceding burst. On the other hand, in the interval $(n-1)/n < \tau < 1$ the number of burst pairs for a particular burst never increases but can decrease by an arbitrary amount from the number of pairs for the preceding burst. The statistics of the two bins are therefore different.

Distributions in τ for burst pairs in the 2B catalog are given in Figure 1. The upper figure gives the distribution of burst pairs for the full 2B catalog; the lower figure gives the distribution for the subset of the 2B catalog with non-MAXBC locations. These histograms have 69 bins covering 691 days, and so the first bin covers 5.00 days. This division of the 2B catalog in τ is chosen because the earlier analysis of Wang & Lingenfelter found a deviation from the average expected value for an interval of 0–5 days in the 1B catalog. The data is plotted as the solid line histogram while the 1σ statistical deviations above and below the average as derived from Monte Carlo simulation are plotted as dotted histograms. A normal distribution gives $\sigma = 50$ in the upper plot and $\sigma = 41$ in the lower plot. The deviations from a normal distribution are substantial, particularly for large τ .

The rate at which BATSE triggers on bursts is highly variable in time due to several factors. First, the trigger is disabled during intervals of the orbit where particle precipitation is a

problem. Second, the burst trigger threshold is raised substantially for 90 minutes after a trigger, which lowers the detection rate of gamma-ray bursts. Third, detector thresholds were changed in response to the transient source GRO J0422+32. Fourth, the fall in the solar flare rate with the approach of the solar maximum lowered the fraction of time the trigger threshold was raised. Finally, excluding bursts with MAXBC locations from the analysis lowers the burst detection rate for the second year of the 2B catalog. The variable burst detection rate makes the average number of bursts expected per unit τ variable. For example, if the detection rate increases linearly so that it is 20% larger at the end of the catalog than at the beginning of the catalog, the distribution in τ will be above average by 0.9% for $\tau = 0$, and it will be below average by 2.2% for $\tau = 1$. Both of these deviations are smaller than the standard deviations of 2% at $\tau = 0$ and 12% at $\tau = 1$. Because the actual change in the detection rate is of this order, rising from an average of 0.81 to 0.88 bursts per day for the full 2B catalog, and falling from 0.81 to 0.60 bursts per day for the non-MAXBC located subset, one sees that the effects of a variable burst detection rate are smaller than the τ -dependent statistical fluctuations.

4. THEORETICAL EXPECTATIONS

The isotropic repeater model has m repeater sources with each source i producing v_i observed outbursts. The distribution of v_i outbursts on the sky around the source position as a consequence of burst location errors is given by

$$\frac{dP_i}{d\Omega} = \frac{v_i}{2\pi\mu(1 - e^{-2/\mu})} e^{-(1 - \cos\theta)/\mu}, \quad (2)$$

where μ is the standard deviation in $1 - \cos\theta$, and is assumed to be the same for all bursts. For $\mu \ll 1$, the position angle error is $\sigma = (2\mu)^{1/2}$. The two-point correlation-function $w(\theta)$ can be solved analytically for this distribution function. Averaged over the interval $x_0 < \cos\theta < x_1$, one has

$$\langle w(\theta) \rangle_{x_0, x_1} = S_{\tau_0, \tau_1} \times \left[\frac{4e^{-2/\mu} \{ \cosh[(2 + 2x_1)^{1/2}/\mu] - \cosh[(2 + 2x_0)^{1/2}/\mu] \}}{(x_1 - x_0)(1 - e^{-2/\mu})^2} - 1 \right], \quad (3)$$

where $S_{\tau_0, \tau_1} = \sum_{i=1}^m v_i(v_i - 1)/N(N-1)$, with N the total number of bursts in the sample.

To apply equation (3) to clustering over the time delay interval τ_0 to τ_1 , we must change S_{τ_0, τ_1} to

$$S_{\tau_0, \tau_1} = \frac{\sum_{i=1}^m \sum_{j=1}^{v_i} n_{i,j}(\tau_0, \tau_1)}{\sum_{i=1}^m N_i(\tau_0, \tau_1)}, \quad (4)$$

where $v_{i,j}(\tau_0, \tau_1)$ is the average number of bursts from source i that fall between τ_0 and τ_1 after burst j and $N_i(\tau_0, \tau_1)$ is the average number of bursts that follow gamma-ray burst i by $\tau_0 < \tau < \tau_1$. Both $v_{i,j}(\tau_0, \tau_1)$ and $N_i(\tau_0, \tau_1)$ are highly model-dependent.

If the time in which a repeater produces all of its bursts is shorter than the time covered by the first bin in τ , then $S_{\tau_0, \tau_1} = 0$ for all bins but the first. In the first bin, the numerator will be $\sum_{i=1}^m v_i(v_i - 1)/2$. If for simplicity we assume that the contribution of the repeaters is negligible to the term in the denomina-

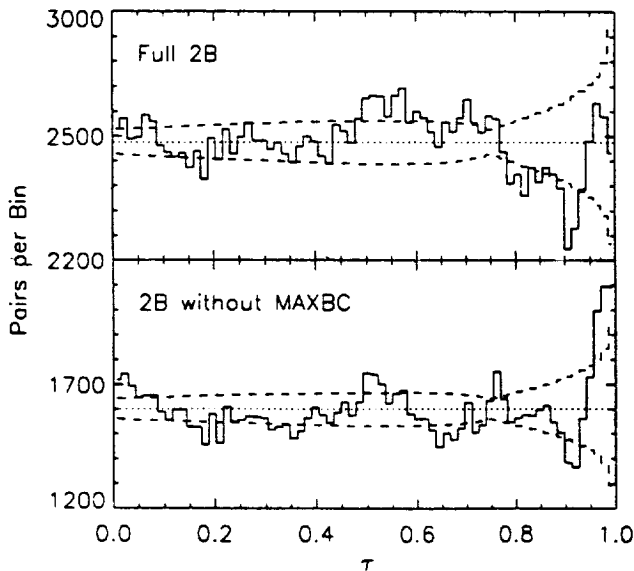


FIG. 1.—Number of bursts in each τ bin. The data are given by the solid line histograms. The data for the full 2B catalog are plotted in the upper diagram, and the data for the subset of bursts with non-MAXBC locations are plotted in the lower diagram. The expected averages are given by the dotted curves and the 1σ statistical deviations are given by the dashed curves.

tor, then the denominator is $\sum_{i=1}^N N_i(\tau_0, \tau_1) \approx \Delta\tau N(N-1)/2$. Therefore in the first bin S_{τ_0, τ_1} is larger than the value found for the full catalog by a factor of $1/\Delta\tau$. Because the statistical fluctuations in the first bin vary approximately as the square root of the number of burst pairs, the signal-to-noise ratio of this signature will rise.

On the other hand, if the bursts from a repeater are randomly distributed, then both the denominator and numerator of S_{τ_0, τ_1} are equal to the values for the full catalog value times $\Delta\tau$, and so the equation for $w(\theta)$ is unchanged. But the statistical noise is worse than for the full catalog, so subdividing over τ decreases the odds of finding clustering.

These two models are the extremes of behavior. A third type of behavior is for all repeaters to have the same period so that periodically spaced bins contain unusually large numbers of pairs of repeater bursts. If m repeaters each produce ν bursts that are periodically spaced over a timescale that is long compared to the width of the time bins, then the numerator of equation (6) is $m(\nu-1)$ for the bins spanning repetition times, and, as with the first example, the signal of repetition increases as the number of time bins increases. But the size of the signal is smaller by a factor of ν from the first example.

The best hope of seeing a clustering in a time-dependent analysis is for it to be in the first time interval.

5. ANALYSIS OF THE 2B CATALOG

Because the statistical fluctuations in the number of burst pairs in an interval $\Delta\tau$ is dependent on τ , the distribution of burst pairs in two-dimensional intervals of $\Delta(\cos\theta)$ and $\Delta\tau$ is highly correlated and not described by a Poisson distribution. However, the distribution over $\cos\theta$ for a particular value of τ is Poisson distributed. As a consequence, the significance of a particular number of bursts in an interval of $\Delta(\cos\theta)$ and $\Delta\tau$ should be determined from the total number of burst pairs in this interval of $\Delta\tau$.

The choice of bin size in $\cos\theta$ is determined by the value of μ in equation (4) set by the BATSE location errors. These errors have a 4° systematic error and a statistical error dependent on the fluence of the burst. Setting $\sigma = 6^\circ$, which describes the error distribution for 85% of bursts, gives $\mu = 0.0055$. Then a choice of 400 bins over the interval $[-1, 1]$ for $\cos\theta$ gives a value of $\langle w(\theta) \rangle_{0.990, 0.995} / \langle w(\theta) \rangle_{0.995, 1} \approx 0.63$. Successive bins fall in value by this factor, so the first three bins contain 83% of the signal. The fourth bin only contains 7% of the signal.

Figure 2a shows for the full 2B catalog the reduced χ^2 of the first ($n=1$) and the first three ($n=3$) bins in $\cos\theta$ for each interval in τ . The same is shown for the subset of 2B bursts with non-MAXBC locations in Figure 2b. The cumulative distribution of the reduced χ^2 of the data is plotted in Figure 3 along with the reduced χ^2 cumulative distribution function. These plots show that only one bin is unusually high, and that is the first bin in $\cos\theta$ covering the interval $0.406 < \tau < 0.420$ (158.3 days $< \Delta T < 164.9$ days) for the full catalog. For 69 bins one expects 0.02 bins to have a fluctuation of this magnitude. But the first three bins in $\cos\theta$ for this time has a reduced χ^2 of 4.7, which is expected for 0.2 bins in a sample of 69 bins. Additional evidence of the statistical origin of the high bin in the upper plot of Figure 1a is that adjacent bins, the bin at a multiple of 2 from the high bin ($0.710 < \tau < 0.725$), and the bins at $0.406 < \tau < 0.420$ in Figure 2b have values expected for an isotropic distribution. The bin covering $0 < \tau < 0.014$ ($0 < \Delta t < 5.0$ days) does not have an exceptionally large devi-

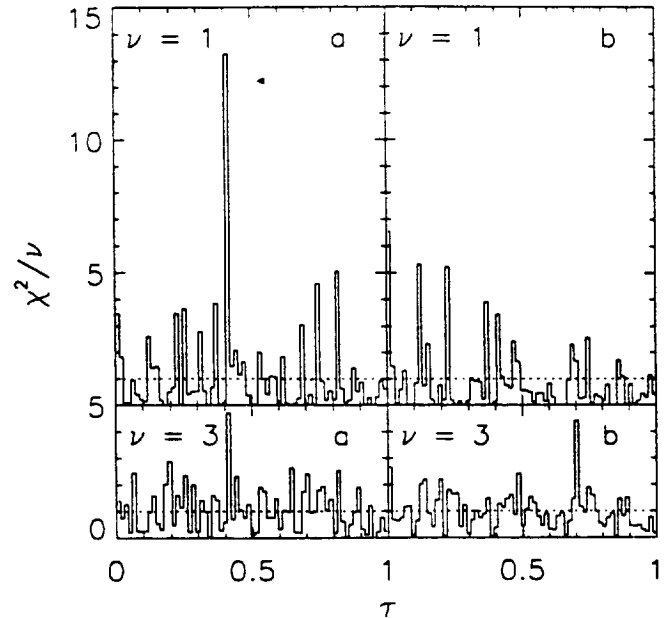


FIG. 2.—Histogram of reduced χ^2 for (a) the full 2B catalog of 585 bursts and (b) the non-MAXBC subset of 485 bursts from the 2B catalog. The upper diagram gives the values of χ^2 for the first bin in $\cos\theta$ ($n=1$). The lower diagram gives $\chi^2/3$ for the first three bins in $\cos\theta$ ($n=3$).

ation in any of the figures. Its largest deviation is for the first bin in $\cos\theta$ in Figure 2b, for which this bin has the largest fluctuation above average of all the bins. But one expects to have 0.7 bins with this large a fluctuation in a sample of 69 bins.

Limits on the value of S_{τ_0, τ_1} are plotted in Figure 4 for each τ bin. These limits are found by applying a modified version of equation (3) to the first three bins in $\cos\theta$ and finding the value

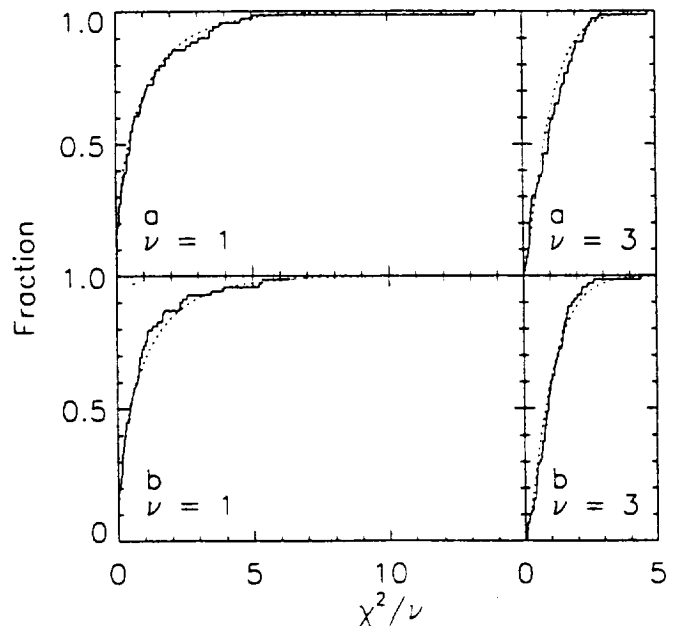


FIG. 3.—Cumulative distribution of reduced χ^2 for the 2B catalog. Labels (a) and (b) are for the data sets described in Fig. 2. The dotted lines give the reduced χ^2 distribution functions.

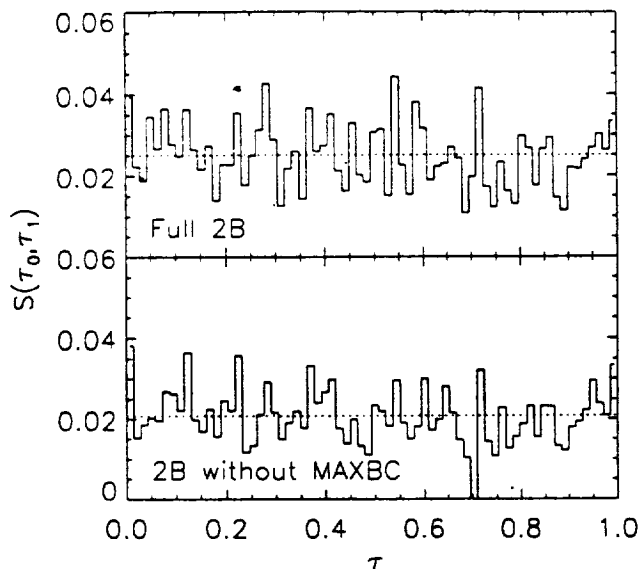


FIG. 4.—Limits on $S(\tau_0, \tau_1)$ of eq. (4). At these limits the probability of a larger reduced χ^2 for the first three bins in $\cos \theta$ is 1%. The bin in the lower diagram that goes to zero has a reduced χ^2 that is below this probability at the χ^2 minimum.

of S_{τ_0, τ_1} that produces a χ^2 of 1% probability. The error model we use is the sum of two Fisher distributions, one with a 6° error and normalized to account for 85% of the bursts, the other with an error of 12° and accounting for the remaining 15% of the bursts. The model is derived from the error distribution of the 2B catalog. The bin at $\tau = 0.7$, which is set to zero, has a χ^2 probability of less than 1% at the minimum value of χ^2 . The average values of S_{τ_0, τ_1} are 0.025 for the full catalog and 0.021 for the subset without MAXBC locations.

The values of S_{τ_0, τ_1} in the first bin are 0.039 for the full catalog and 0.038 for the burst subset.

The full catalog produces a total of 2528 burst pairs over the first time bin, so for a model in which all observed repetitions from a source occurs within 5 days of the first burst, the upper limit on the number of sources appearing in the full catalog as repeaters is $m < 197/v(v-1)$ at the 99% confidence level, where we have assumed that each identifiable repeating source produced v observed bursts. For $v = 3$, this implies that the fraction of observed bursts that are from identifiable repeaters is $f = mv/N < 0.17$. For $v = 2$ this limit rises to $f < 0.34$. The non-MAXBC located bursts produce 1818 burst pairs in the first time bin, which gives a limit on identifiable repeater sources of $m < 138/v(v-1)$ at the 99% confidence level. For $v = 3$ one has $f < 0.14$, and for $v = 2$, $f < 0.28$. From these limits on the data one can derive model-dependent limits on the fraction of burst sources producing multiple observed and unobserved bursts. For repeaters producing 2, 3, 4, 6, 8, and 10 outbursts the upper limits on the fraction of repeating sources in the full catalog are 85%, 22%, 9.8%, 3.6%, 1.8%, and 1.1%, with the average number of observed bursts from identifiable repeaters ranging from 2 to 3.9. For the non-MAXBC located bursts, the 2 outburst repeater model has a formal upper limit on the repeater source fraction of 103% at the 99% confidence level, and therefore no physical upper limit, and the models with 3, 4, 6, 8, and 10 outbursts have upper limits on the repeater source fraction of 25%, 11%, 4.0%, 2.1%, and 1.3%, with the average number of bursts observed from identifiable repeaters ranging from 2.1 to 3.3.

We find no evidence of burst repetition in either the full 2B catalog or the subset of this catalog with non-MAXBC locations.

This work is supported by NASA contract NAG 5-2056.

REFERENCES

- Blumenthal, G.-R., Hartmann, D. H., & Linder, E. V. 1994, in Proc. Gamma-Ray Bursts: 2d Workshop, ed. G. J. Fishman, J. J. Brainerd, & K. Hurley (New York: AIP), 117
- Briggs, M. S., Paciesas, W. S., Pendleton, G. N., Fishman, G. J., Meegan, C. A., Horack, J. M., Brock, M. N., Kouveliotou, C., Hartmann, D. H., & Hakkila, J. E. 1995, *ApJ*, submitted
- Hakkila, J. E., Meegan, C. A., Pendleton, G. N., Fishman, G. J., Wilson, R. B., Paciesas, W. S., Brock, M. N., & Horack, J. M. 1994, *ApJ*, 422, 659
- Meegan, C. A., et al. 1994, Basic Information Table of the BATSE 2B Gamma-Ray Burst Catalog [electronic catalog]; available from grossc.gsfc.nasa.gov; Internet user name gronews
- Meegan, C. A., Hartmann, D. H., Brainerd, J. J., Briggs, M. S., Paciesas, W. S., Pendleton, G. N., Kouveliotou, C., Fishman, G. J., Blumenthal, G., & Brock, M. N. 1995, *ApJL*, submitted
- Quashnock, J. M., & Lamb, D. Q. 1993, *MNRAS*, 265, L59
- Wang, V., & Lingenfelter, R. E. 1993, *ApJ*, 416, L13
- . 1994, in Proc. Gamma-Ray Bursts: 2d Workshop, ed. G. J. Fishman, J. J. Brainerd, & K. Hurley (New York: AIP), 160

MIMICKING WITHIN EUCLIDEAN SPACE A COSMOLOGICAL TIME DILATION OF GAMMA-RAY BURST DURATIONS

J. J. BRAINERD¹

University of Alabama in Huntsville, Department of Physics, Huntsville, AL 35899
 E-mail: brainerd@ssl.msfc.nasa.gov.

Received 1994 February 22; accepted 1994 March 22

ABSTRACT

If gamma-ray burst sources are cosmological in origin, then the time dilation at large z can correlate a burst's duration with its peak flux. Detection of this effect is thought by many to be strong evidence for a cosmological burst origin. In this *Letter* I show that an apparent time distortion—either a dilation or contraction—is generally expected for an ensemble of bursts that is spatially limited within Euclidean space. The appearance of this effect is correlated with the falling away of the $\log N$ – $\log P$ curve from a $-3/2$ slope line. An example of this effect is provided by the relativistic bulk motion model, which produces a strong time dilation when spatially limited in Euclidean space. As a consequence, evidence that weak bursts have longer durations than strong bursts is not evidence of a cosmological burst origin.

Subject headings: gamma-rays; bursts

1. INTRODUCTION

Cosmological models of gamma-ray bursts are slowly superseding the older galactic models within the theoretical astrophysics community, but this shift is based on only one observational result: the isotropic but inhomogeneous distribution of gamma-ray bursts. This is somewhat unsatisfying in that the evidence is against a galactic origin rather than for a cosmological origin.

Finding positive evidence for a cosmological origin is quite difficult: no gamma-ray burst has a line from which a redshift can be derived; no gamma-ray burst has a gravitational lens associated with it; and no gamma-ray burst has a quiescent counterpart from which to derive a distance. This forces one to search for cosmological signatures in burst ensembles. The difficulty of such an undertaking was recently emphasized by Trimble (1994), who pointed out that in studies of extragalactic sources evolution dominates cosmological expansion.

Over the past several years a number of authors have proposed finding a cosmological redshift in gamma-ray bursts by studying their temporal structure (Paczynski 1992; Piran 1992). Essentially these studies attempt to discover whether weak bursts are on average longer than strong bursts, since cosmological time dilation produces such an effect. Recently several authors claimed to find this correlation between duration and flux from several different tests applied to data from the Burst and Transient Source Experiment (BATSE) on board the *Compton Gamma-Ray Observatory* (CGRO) (Norris et al. 1993, 1994; Davis et al. 1994), although others fail to find the effect after applying one of these tests to a different BATSE data set (Mitrofanov et al. 1994).

In § 2 of this letter I show that the observation of a lengthening burst duration with decreasing flux is easily produced by an inhomogeneous distribution of bursts in Euclidean space. Moreover, the flux at which the time dilation appears is also the flux below which the $\log N$ – $\log P$ curve deviates from a $-3/2$ power-law. As a consequence, an

observed onset of time dilation at fluxes below the break in the $\log N$ – $\log P$ is not evidence that burst sources are cosmological rather than galactic. I clarify this point in § 3 by calculating the average duration as a function of minimum flux for a relativistic bulk motion model of gamma-ray bursts. My conclusions regarding our inability to determine the origin of bursts through the average characteristics of burst ensembles are given in § 4.

2. TIME-FLUX DEPENDENCE IN EUCLIDEAN SPACE

If gamma-ray bursts are confined to Euclidean space, then there is no fundamental link between the distance at which the burst density goes to zero and a dilation of burst duration. In what follows I assume that the intrinsic characteristics of gamma-ray bursts are independent of their position in space. I also assume, to simplify the problem, that bursts are isotropically distributed about the earth with a density $n(r)$. This density goes to a constant value for $r \ll r_c$, where r_c is a characteristic length scale, and it rapidly goes to 0 as $r \rightarrow \infty$ (that is, sufficiently fast to make the integrals defined below bounded). The distribution function for the parameters characterizing a gamma-ray burst is defined as $G(q)$, where q is an n -dimensional vector of all burst parameters, such as the intrinsic duration and the intrinsic peak flux.

The various timescales measured by the various proposed tests can be represented as the average over the burst duration t . This is given by the following ratio of integrals:

$$\langle t \rangle = \frac{\int_V t G(q) n(r) r^2 dr d^n q}{\int_V G(q) n(r) r^2 dr d^n q}, \quad (1)$$

where V represents the integral over all observable parameter space. The peak flux of a burst is defined by $f = F(q)/r^2$. Because a burst is observed when $f > f_0$, one sees that any value of q produces an observable burst for some value of r as long as $F(q) \neq 0$. As a consequence, only r has an integration limit that is less than its full range of variation. This integral is

$$\int_0^{r_0} n(r) r^2 dr = N(r_0), \quad (2)$$

¹ Postal address: Space Science Lab, ES-84, NASA Marshall Space Flight Center, Huntsville, AL 35812.

where

$$r_0 = \sqrt{\frac{F(q)}{f_0}}. \quad (3)$$

The observed time is also a function of the intrinsic characteristics of the burst, and can be written as $t = T(q)$. With these definitions, the observed average duration is given by

$$\langle t \rangle = \frac{\int_{V_q} T(q) G(q) N(\sqrt{F(q)/f_0}) d^n q}{\int_{V_q} G(q) N(\sqrt{F(q)/f_0}) d^n q}. \quad (4)$$

The integrals are over the full domain of q .

Two important facts are immediately apparent from this equation. The first is that if the burst density is constant throughout Euclidean space to infinity, then $N(r) \propto r^3$, and f_0 factors out of equation (4), making the average duration independent of the limiting flux. This implies that the bursts in the $-3/2$ portion of the log $N - \log P$ curve should show no evidence of a correlation of duration with peak flux, and therefore no evidence of a time dilation.

The second important fact is that for a general function of $N(r)$ the limiting flux cannot be factored out, so the only way of removing the dependence of $\langle t \rangle$ on f_0 is to let $G(q) = g(q_1)h(q_2)$, where q_1 and q_2 are independent subsets of q , with $T(q) = T(q_1)$ and $F(q) = F(q_2)$. In this case equation (4) becomes

$$\langle t \rangle = \int T(q_1) g(q_1) d^n q_1 / \int g(q_1) d^n q_1,$$

which is independent of f_0 . But if this separation is impossible—and generally it is—one must expect $\langle t \rangle$ to have a dependence on f_0 whenever one is observing to the spatial limit of sources. This implies that one should expect to observe a time dilation or contraction when comparing the average duration of bright bursts to the average duration of dim bursts. If one is unlucky, it will be a dilation, which could mimic the time dilation expected for a Friedmann universe.

3. THE RELATIVISTIC BULK MOTION MODEL

It is, in fact, easy to be unlucky in our models. As an example I examine a relativistic bulk motion model for gamma-ray bursts, which has long been a staple of galactic models, and is now used in most cosmological models. In this model a burst's intrinsic duration τ and intrinsic luminosity are set in the co-moving frame of the medium emitting the gamma-rays. For a Lorentz factor of γ , a dimensionless momentum u ($\gamma^2 = 1 + u^2$), and an emission angle θ relative to the direction of motion as measured in the observer's inertial frame, the observed duration t is

$$t = \frac{\tau}{\gamma} (\gamma - u \cos \theta). \quad (5)$$

The observed photon number flux f within a fixed spectral band for a power-law photon spectrum of index $-\delta$ is

$$f = \frac{F_0}{r^2} (\gamma - u \cos \theta)^{-2-\delta}, \quad (6)$$

where F_0 is a constant proportional to the intrinsic burst luminosity.

The model we shall examine is composed of mono-energetic gamma-ray burst sources that are uniformly distributed within a sphere of radius R . Because u , δ , and F_0 are fixed in value, the jet orientation, which is uniformly distributed over 4π , is the

only free variable. Defining $\mathcal{F}_0 = f_0 R^2 / F_0$, equation (4) becomes

$$\langle t \rangle = \frac{\tau}{\gamma} \frac{\int_{-1}^1 (\gamma - u \cos \theta) N[\mathcal{F}_0^{-1/2} (\gamma - u \cos \theta)^{-1-(\delta/2)}] d \cos \theta}{\int_{-1}^1 N[\mathcal{F}_0^{-1/2} (\gamma - u \cos \theta)^{-1-(\delta/2)}] d \cos \theta}. \quad (7)$$

The function $N(r)$ is Cr^3 for $r < R$ and CR^3 for $r \geq R$, where C is a constant. Evaluating the integrals in equation (7) under the assumption that $\gamma - u \ll 1$ gives the following approximate result:

$$\langle t \rangle = \frac{\tau}{\gamma} \frac{3\delta + 4}{3\delta + 2} \times \begin{cases} \frac{1}{\gamma + u}, & \text{if } \mathcal{F}_0 > (\gamma + u)^{\delta+2}; \\ \mathcal{F}_0^{-1/(\delta+2)} \frac{2 + (3\delta + 2)[1 - \mathcal{F}_0^{1/(\delta+2)}(\gamma - u)]}{2 + (3\delta + 4)[1 - \mathcal{F}_0^{1/(\delta+2)}(\gamma - u)]}, & \text{otherwise.} \end{cases} \quad (8)$$

A normalized version of this equation is plotted in Figure 1 for $\delta = 1, 2$, and 4 . From equation (8) one sees that the average time is constant for $\mathcal{F}_0 > (\gamma + u)^{\delta+2}$ and proportional to $\mathcal{F}_0^{-1/(\delta+2)}$ for $\mathcal{F}_0 \ll (\gamma + u)^{\delta+2}$. If the underlying spectrum of the burst is hard (i.e., $\delta \approx 2$), the average length of the burst increases as $\mathcal{F}_0^{-1/4}$, which gives a factor of 1.8 increase in duration with each factor of 10 decrease in burst flux.

The log $N - \log \mathcal{F}_0$ curve is given by

$$N \propto u^{-1} \begin{cases} (\gamma + u)^{3\delta+4/2} \mathcal{F}_0^{-3/2}, & \text{if } \mathcal{F}_0 > (\gamma + u)^{\delta+2}; \\ \mathcal{F}_0^{-1/(\delta+2)} \left\{ 1 + \frac{3\delta + 4}{2} [1 - \mathcal{F}_0^{1/(\delta+2)}(\gamma - u)] \right\}, & \text{otherwise.} \end{cases} \quad (9)$$

A normalized version of this equation is plotted in Fig. 2.

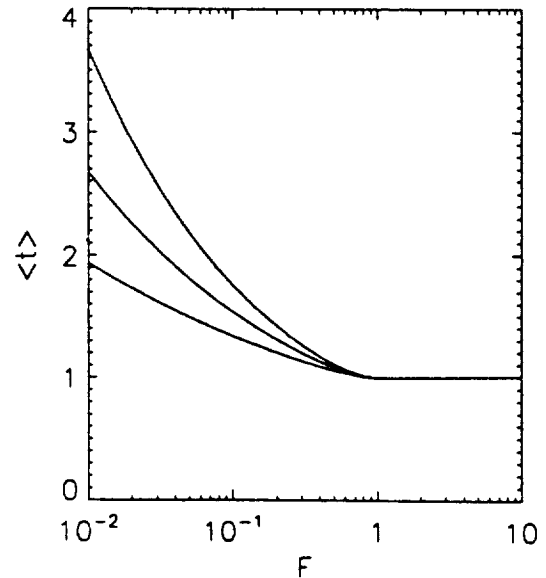


FIG. 1.—Average burst duration vs. the minimum peak flux for the relativistic bulk motion model. The minimum peak flux is defined as $F = \mathcal{F}_0/(\gamma + u)^{\delta+2}$, and the average burst duration $\langle t \rangle$ is normalized to unity for $F > 1$. From top to bottom the curves have $\delta = 1, 2$, and 4 .

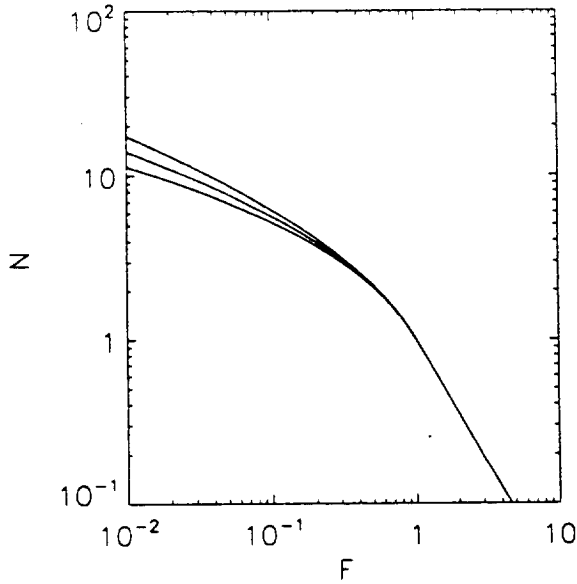


FIG. 2.—Log $N - \log F$ curves of the relativistic bulk motion model. The peak flux F is defined as in Fig. 1, and the cumulative burst number N is normalized to unity at $F = 1$. From top to bottom the curves have $\delta = 1, 2$, and 4.

Comparing equations (8) and (9) (or Figs. 1 and 2), one sees that the appearance of the break in the $\log N - \log F$ is tied to the appearance of a time dilation.

Because the slope of the $\log N - \log F_0$ is order of $-\frac{1}{2}$, the observed break to ≈ -0.8 (Meegan et al. 1994) must be constructed by allowing u and F_0 to vary. Each variable affects the average observed duration in a different manner, which suggests that one can easily construct a model that is consistent with the observations. For example, if the distribution of u is u^α for $u < u_0$, and 0 for $u > u_0$, then the resulting $\log N - \log f$ curve breaks to a slope of $(\alpha - 1)/(\delta + 2)$ as $f \rightarrow 0$. This gives a slope of -0.83 when $\alpha = -1.5$ and $\delta = 1$. This distribution produces a much stronger time dilation for the weak bursts than is shown in Figure 1 ($\langle t \rangle = 3.6$ at $F = 10^{-2}$ for the $\delta = 2$ curve with $\alpha = -1.5$), with the average duration going to

$f^{-2/(\delta+2)}$ as $f \rightarrow 0$. On the other hand, if the intrinsic luminosity has a distribution function of F_0^β for $F_0 \leq F_c$ and 0 for $F_0 > F_c$, then the $\log N - \log f$ curve breaks to a slope of $\alpha + 1$. The time dilation for this distribution is much weaker than in Figure 1 ($\langle t \rangle = 1.3$ at $F = 10^{-2}$ for the $\delta = 2$ curve with $\alpha = -1.8$), going to a constant for $\alpha < -1 - 2/(\delta + 2)$ as $f \rightarrow 0$.

4. CONCLUSIONS

Whether or not a given characteristic measured for an ensemble of gamma-ray bursts is strong evidence for a particular burst model depends on the uniqueness of the result. As the above discussion indicates, the appearance of time dilation in bursts with fluxes below the break in the $\log N - \log P$ curve from the $-3/2$ slope is not unique to cosmological models, but is in fact expected for some noncosmological models. As a consequence, the results of Norris et al. (1993, 1994) and Davis et al. (1994) are consistent with, but not proof of, a cosmological origin of gamma-ray bursts.

The intrinsic properties of current cosmological burst models may dominate any effect from cosmological expansion. The reason is that all models now under consideration employ bulk relativistic motion to avoid the destruction of the observed GeV photons through photon-photon pair creation. If the bulk motion is only in one direction, a correlation of burst duration with burst flux appears. One must keep in mind that this effect is strong, and therefore may compete with any cosmological redshift.

These comments concerning time dilation also apply to the dependence of the average peak value of the vF_ν curve on the minimum burst flux and to other measures of spectral curvature. The general nature of equation (4) suggests that studies of the average characteristics of gamma-ray bursts will not resolve the question of burst origin, and that we must look to other tests, such as the discovery of gravitationally lensed gamma-ray bursts (Nemiroff et al. 1994) or the observation of photoelectric absorption of bursts at low galactic latitude (Schaefer 1993, 1994), for model-independent derivations of the distance to gamma-ray bursts.

This work is supported by NASA grant NAS8-38609.

REFERENCES

- Davis, S. P., Norris, J. P., Kouveliotou, C., Fishman, G. J., Meegan, C. A., & Paciesas, W. S. 1994, in *Gamma-Ray Bursts: Huntsville, 20–22 October, 1993*, ed. G. J. Fishman, J. J. Brainerd, & K. C. Hurley (New York: AIP), in press
- Meegan, C. A., et al. 1994, in *Gamma-Ray Bursts: Huntsville, 20–22 October, 1993*, ed. G. J. Fishman, J. J. Brainerd, & K. C. Hurley (New York: AIP), in press
- Mitrofanov, I. G., Cherenko, A. M., Pozanenko, A. S., Paciesas, W. S., Kouveliotou, C., Meegan, C. A., Fishman, G. J., & Sagdeev, R. Z. 1994, in *Gamma-Ray Bursts: Huntsville, 20–22 October, 1993*, ed. G. J. Fishman, J. J. Brainerd, & K. C. Hurley (New York: AIP), in press
- Nemiroff, R. J., Wickramasinghe, W. A. D. T., Norris, J. P., Kouveliotou, C., Fishman, G. J., Meegan, C. A., & Paciesas, W. S. in *Gamma-Ray Bursts: Huntsville, 20–22 October, 1993*, ed. G. J. Fishman, J. J. Brainerd, & K. C. Hurley (New York: AIP), in press
- Norris, J. P., Nemiroff, R. J., Kouveliotou, C., Fishman, G. J., Meegan, C. A., Wilson, R. B., & Paciesas, W. S. 1993, in *Compton Gamma-Ray Observatory: St. Louis, MO 1992*, ed. M. Friedlander, N. Gehrels, & D. J. Macomb (New York: AIP), 947
- Norris, J. P., Nemiroff, R. J., Scargle, J. D., Kouveliotou, C., Fishman, G. J., Meegan, C. A., Paciesas, W. S., & Bonnell, J. T. 1994, *ApJ*, 424, 540
- Paczynski, B. 1992, *Nature*, 355, 521
- Piran, T. 1992, *ApJ*, 389, L45
- Schaefer, B. E. 1993, in *Compton Gamma-Ray Observatory: St. Louis, MO 1992*, ed. M. Friedlander, N. Gehrels, & D. J. Macomb (New York: AIP), 803
- . 1994, in *Gamma-Ray Bursts: Huntsville, 20–22 October, 1993*, ed. G. J. Fishman, J. J. Brainerd, & K. C. Hurley (New York: AIP), in press
- Trimble, V. 1994, in *Gamma-Ray Bursts: Huntsville, 20–22 October, 1993*, ed. G. J. Fishman, J. J. Brainerd, & K. C. Hurley (New York: AIP), in press

A STUDY OF THE EFFECTS OF BACKGROUND SUBTRACTION ON OCCULTATION IMAGING

W. S. PACIESAS

*University of Alabama in Huntsville
Huntsville, AL 35899 USA*

and

S. N. ZHANG*, B. C. RUBIN*, B. A. HARMON and G. J. FISHMAN

*NASA/Marshall Space Flight Center
Huntsville, AL 35812 USA*

Abstract. One of the crucial steps in the occultation transform imaging technique involves the removal of the time-varying instrumental background. Previous versions of this imaging technique applied to BATSE data have used simple high-pass filtering to eliminate background variations on timescales longer than the typical duration of an occultation step (of order 10 s). We have investigated an alternative technique in which the imaging algorithm is applied to the residuals generated from fitting the raw data with a semi-empirical model of the background. Comparison of the resulting maps shows that the latter does not significantly improve imaging performance.

Key words: X-Rays: Imaging – X-Rays: Background Studies

1. Introduction

Though observations of gamma-ray bursts are its primary objective, BATSE has considerable capabilities as a hard X-ray all-sky monitor. Pulsed sources may be detected by BATSE using Fourier and/or summed epoch analysis, and any type of source may be detected by Earth occultations, *i.e.*, measuring the difference in background rate between times when a source is visible and times when it is occulted by the Earth. The usefulness of BATSE for monitoring was increased substantially when we developed the method of occultation transform imaging [1, 2] which allows us to obtain more accurate positional information on transient sources and to discriminate better among sources in crowded regions. An overview of the imaging methodology is given elsewhere in these proceedings [3]. Here we describe the necessity for, and implementation of, background subtraction when producing images.

2. Background Effects in Occultation Imaging

Occultation imaging is possible only to the extent that the variations due to a source rising or setting may be distinguished from the time variability of the background due to other effects (*e.g.*, electron precipitation, cosmic ray

* also Universities Space Research Association

latitude dependence, solar flares, SAA activation). In the case of BATSE, these variations generally fall into one of two categories: 1) intermittent fluctuations on timescales shorter than, or comparable to, the duration of an occultation step, or 2) more regular, longer-timescale variations.

In practice, we remove the two different types of background fluctuations by different methods. The short timescale fluctuations are intermittent and relatively rare. These are quite effectively removed by visual scanning of the data: periods of activity on these timescales are flagged as part of daily BATSE operations and removed from subsequent occultation analysis. The longer timescale fluctuations are more difficult because they are ubiquitous, depending on the combined effects of the cosmic diffuse and atmospheric backgrounds, trapped cosmic rays, SAA activation, etc., whose relative contributions depend on energy as well as spacecraft position. During the initial development of the occultation imaging software, the available background models were not sufficiently mature to be useful, so a simple differentiation was applied to the data and the results modeled by the Radon transform [1, 2]. These early images clearly showed the usefulness of the technique and stimulated us to look for ways to improve the sensitivity.

One of the first significant improvements was to eliminate the simple differentiation scheme in favor of a high-pass filter to eliminate the lower frequency background components. Fig. 1 illustrates the effectiveness of this methodology. The uppermost curve in the figure shows slightly more than two orbits of raw data (1.024 s resolution) from a single BATSE detector. Gaps in the data are evident, typically resulting from either transmission errors, South Atlantic Anomaly passages, or filtering of short-timescale fluctuations. The next lower curve shows the same data with gaps filled in by a simple linear interpolation. The bottom two curves compare the data after differentiation (upper) with the data after application of a second order high-pass Butterworth filter (lower). Comparison of the lowest curve with the idealized point source signal (see Fig. 1 of ref. [3]) shows the obvious improvement in signal-to-noise for filtered *vs.* differentiated data.

In parallel with the development of occultation imaging, we have been developing semi-empirical background models for eliminating the longer timescale background variations [4, 5]. Fitting of the model described in Ref. [4] is now being performed daily as part of routine BATSE operations. The output files produced include not only the model terms but also the full set of data residuals.

3. Comparison of Images

It is natural to consider whether the use of a proper background model would further improve the occultation imaging relative to the simpler high-pass filter. Thus, we embarked on the present study to compare the two methods.

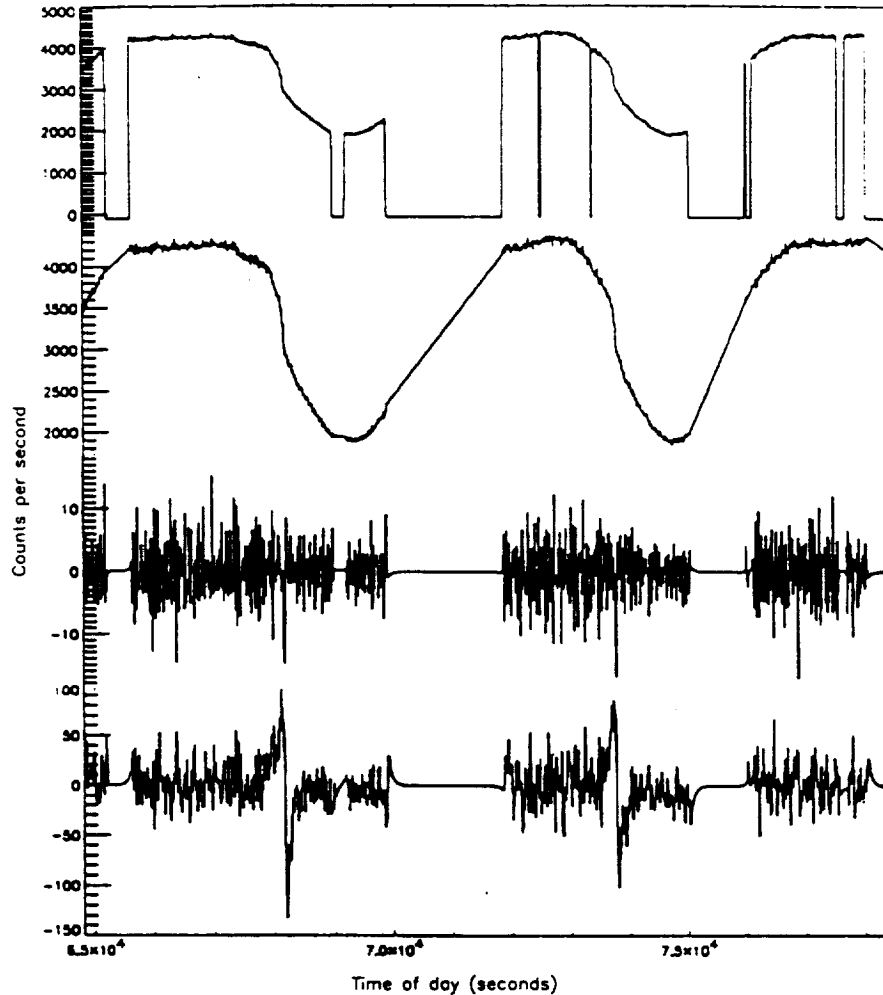


Fig. 1. Example of data treatment for occultation transform imaging. The uppermost pair of curves show raw BATSE data with gaps present and with gaps filled in, respectively. The lowermost pair of curves show the same data after differentiation and high-pass filtering, respectively.

We generated images of selected regions using both our standard imaging software which includes the Butterworth high-pass filter and a modified version which bypasses the filter and uses the background model residual files. Subtraction of the background model has the same effect on the point source signal as the high-pass filter; hence, the same mapping algorithm can be applied to both cases. Fig. 2 shows a typical result, in this case single-day images of a region in Scorpius which includes a strong source, the recent X-ray nova [6, 7]. The filtered image is slightly better in that it converges to a single source; however, the two images are effectively the same.

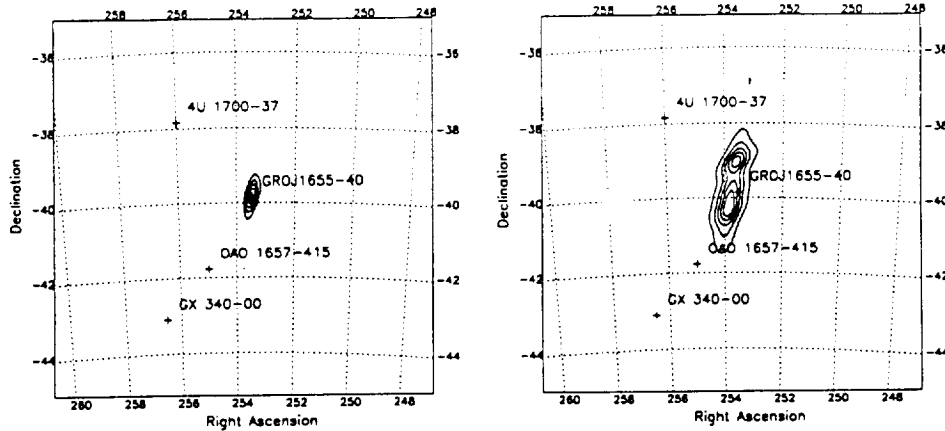


Fig. 2. Images of Nova Scorpii 1994 on TJD 9575. The left hand image was produced with the high-pass filter; the right hand image was produced from the background model residuals.

We made additional comparisons for several different sky regions having a range of source intensities. Although some small differences were evident as in Fig. 2, we found no consistent reason to favor either method.

4. Conclusions

For the current occultation imaging methodology, there is no advantage to using the semi-empirical background model. The images produced using the Butterworth filter, which is computationally less intensive, are at least as good as the images produced from the model fit residuals. Given this performance, we are implementing a similar high-pass filter in our other occultation software packages. We expect that this will significantly improve the BATSE sensitivity for detection and flux determination of hard X-ray and low-energy gamma-ray sources.

References

1. Zhang, S.N. *et al.*: 1993, *Nature* **366**, 245
2. Zhang, S.N. *et al.*: 1994, *IEEE Trans. Nucl. Sci.* **41**, 1313
3. Zhang, S.N. *et al.*: 1995, these proceedings
4. Rubin, B.C. *et al.*: 1993, in M. Friedlander, N. Gehrels & D.J. Macomb, eds., *Compton Gamma-Ray Observatory*, AIP: New York, 1127
5. Skelton, R.T. *et al.*: 1993, in M. Friedlander, N. Gehrels & D.J. Macomb, eds., *Compton Gamma-Ray Observatory*, AIP: New York, 1189
6. Zhang, S.N. *et al.*: 1994, IAU Circ. No. 6046
7. Wilson, C.A. *et al.*: 1994, IAU Circ. No. 6056

DISCOVERY OF A NEW X-RAY TRANSIENT IN SCORPIUS

GRO J1655-40 \equiv X-ray Nova Scorpii 1994

W.S. PACIESAS

*University of Alabama in Huntsville
Huntsville, AL 35899 USA*

S.N. ZHANG AND B.C. RUBIN

*Universities Space Research Association
Huntsville, AL 35806 USA*

AND

B.A. HARMON, C.A. WILSON AND G.J. FISHMAN

*NASA/Marshall Space Flight Center
Huntsville, AL 35812 USA*

Abstract. A bright transient X-ray source, GRO J1655-40 (X-ray Nova Scorpii 1994) was discovered with BATSE (the Burst and Transient Source Experiment) in late July 1994. More recently, the source also became a strong radio emitter, its rise in the radio being approximately anti-correlated with a decline in the hard X-ray intensity. High-resolution radio observations subsequent to this symposium showed evidence for superluminally expanding jets. Since the hard X-ray emission extends to at least 200 keV and we find no evidence of pulsations, we tentatively classify the source as a black-hole candidate. However, its hard X-ray spectrum is unusually steep (power-law photon index $\alpha \simeq -3$) relative to most other black-hole candidates. In this regard, it resembles GRS 1915+105, the first galactic source to show superluminal radio jets.

1. Introduction

GRO J1655-40 (also designated X-ray Nova Sco 1994) was first detected with BATSE (Zhang *et al.* 1994a) on 27 July 1994 and located initially to within about 0.3° using Earth occultation imaging (Zhang *et al.* 1993). A candidate optical counterpart was found by Bailyn *et al.* (1994) and confirmed spectroscopically by Della Valle (1994). Subsequently, we used additional BATSE data to produce an improved location (Wilson *et al.* 1994),

with a precision of about 0.1° , which agreed well with the optical counterpart.

The radio counterpart to GRO J1655-40 was first detected on 6 August by Campbell-Wilson & Hunstead (1994a) who used the Molonglo Observatory Synthesis Telescope (MOST). From its initial intensity of 370 mJy at 843 MHz, the source continued to flare, reaching more than 5 Jy on 15 August Campbell-Wilson & Hunstead (1994b). It quickly became apparent that this radio source was unusually bright in comparison with other X-ray transients. The radio spectrum during most of the rise was consistent with optically-thick synchrotron emission (Hjellming 1994a). The early radio observations are described in more detail in an accompanying paper (Hunstead *et al.* 1995).

Subsequent to this symposium, the radio intensity peaked at ~ 7 Jy around 17-18 August and the spectrum became optically thin (Hunstead *et al.* 1994). The source was the subject of an intensive campaign of interferometric radio observations. The initial observations showed a double source with the components moving apart (Hjellming 1994b). At an estimated distance of ~ 3.5 kpc (McKay & Kesteven 1994), the apparent separation velocity is superluminal (Reynolds & Jauncey 1994; Hjellming & Rupen 1994a). BATSE observed further X-ray outbursts in September (Paciesas *et al.* 1994) and November (Zhang *et al.* 1994b,c), with associated radio activity (Hjellming & Rupen 1994b,c,d). The hard X-ray, radio and optical behavior of X-ray Nova Sco 1994 is summarized elsewhere (Harmon *et al.* 1995; Hjellming & Rupen 1995; Tingay *et al.* 1995; Bailyn *et al.* 1995).

2. Observations

The early history of GRO J1655-40 was remarkable for its unusually fast rise. Figure 1 shows the hard X-ray intensity derived from Earth occultation measurements using BATSE. We show data from individual source rises and sets in order to provide the best possible time resolution using this technique. The first clear detection of the source occurs around the end of 27 July and the turn-on occurs in less than 0.5 days, and may be as short as 0.25 days. There is a weak indication of emission for several days prior to the turn-on, but this may be a systematic effect, possibly due to interference from nearby sources such as the variable X-ray pulsar OAO 1657-415.

The occultation geometry for several days around the turn-on of GRO J1655-40 was particularly unfavorable for separation of this source from the OAO pulsar. The latter had been detected in a bright state since mid-June by the BATSE daily epoch-folding search. However, the midpoint of its binary eclipse occurred on 27 July and pulsations were not detected by BATSE on either that day or the following day. Furthermore,

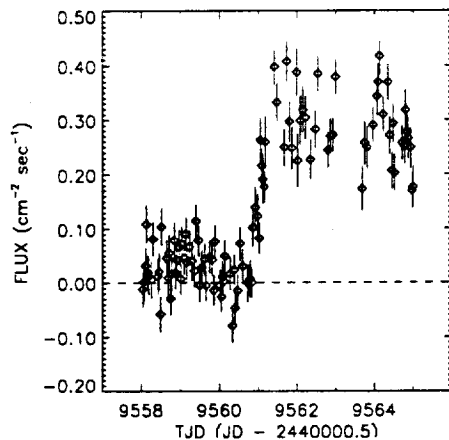


Figure 1. The early intensity history of GRO J1655-40 derived from individual occultation steps. The energy range is 20-430 keV. The rise begins around the end of Truncated Julian Day (TJD) 9560 (27 July) and the turn-on to essentially full intensity occurs in less than 0.5 day.

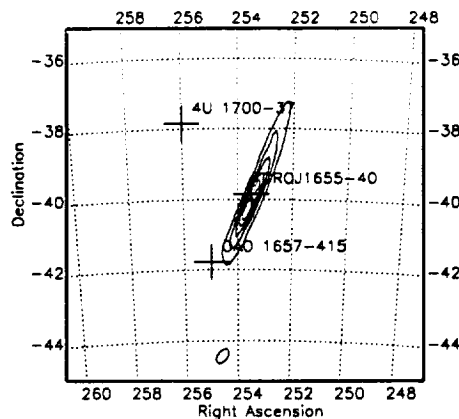


Figure 2. Occultation transform image for 30 July showing the region surrounding GRO J1655-40. The dominant emission is clearly distinct from the nearby X-ray pulsar OAO 1657-415. Due to the unfavorable occultation geometry the contours are severely elongated along the direction of the Earth's limb.

occultation images of the region showed that the new source was clearly distinct from the OAO source. Figure 2 shows one such image for 30 July. The effect of the unfavorable occultation geometry is evident in the elongated contours. The OAO source is not visible in the image even though it was detected on this day by the BATSE epoch-folding and Fast Fourier Transform (FFT) searches which are more sensitive than the occultation method for detecting pulsed sources.

The lack of any significant unidentified peaks in the FFT search allows us to place an upper limit of $\sim 10\%$ on the pulsed fraction in the 20-100 keV band at maximum intensity, indicating that the new source is likely to be a black-hole candidate. We also generated power spectra of the data during the times when the source was visible to look for excess red noise or flickering. No obvious evidence of flickering was detected; however, a more detailed investigation is in progress (Crary *et al.* 1995).

The intensity history of GRO J1655-40 as of the time of this symposium is shown in Fig. 3. Here we have averaged the data in intervals of up to one day and we have omitted data from days when the interference from OAO 1657-415 was most severe. In contrast to most other such transients, the light curve of this source is erratic, showing no clear trend until the rather fast intensity drop around 13 August. Superimposed on Fig. 3 we also show the radio intensity, which increased spectacularly around the time

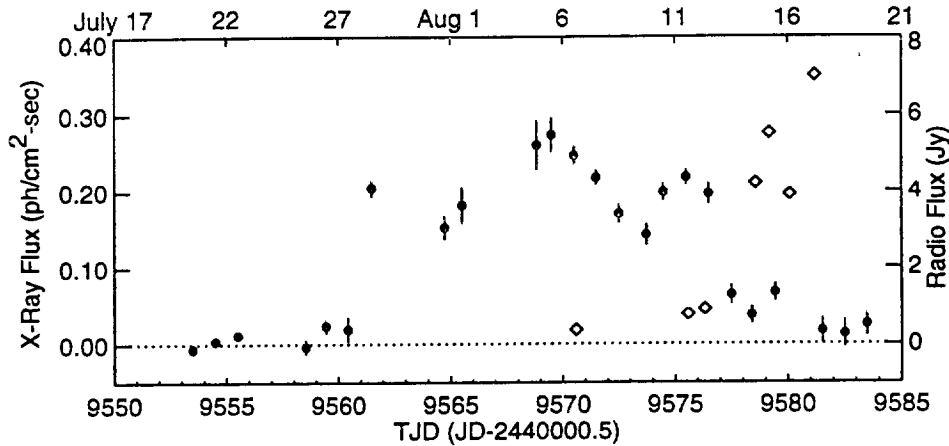


Figure 3. The intensity history of the entire initial outburst of GRO J1655-40. The energy range is 20-100 keV and the data points (solid circles) are one-day averages. The indicated errors are statistical only. Diamonds show the radio intensity at 843 MHz (Campbell-Wilson & Hunstead 1994a,b; Hunstead *et al.* 1994).

of the hard X-ray drop.

Preliminary analysis showed that the GRO J1655-40 hard X-ray spectrum was fit adequately with a single power law, with some evidence for hardening with time. We obtained values of the photon index $\alpha = -3.38 \pm 0.07$ ($\chi^2 = 18.1$ for 18 d.o.f.) during 1-4 August and $\alpha = -2.95 \pm 0.06$ ($\chi^2 = 66.8$ for 38 d.o.f.) during 4-8 August. We find no evidence for the high-energy cut-off typically seen in the spectra of black-hole candidates (Sunyaev *et al.* 1991). In fact, nearly contemporaneous observations using the OSSE instrument on CGRO detect emission to at least 600 keV (Kroeger *et al.* 1994) and in comparison with the BATSE results suggest a spectral flattening at higher energies. In the OSSE energy range ($E > 50$ keV), Kroeger *et al.* (1994) measured $\alpha = -2.7$ on 4 August and $\alpha = -2.4$ on 9 August.

3. Discussion

Although it is tempting to classify GRO J1655-40 as a black-hole candidate, it is somewhat unusual among unpulsed hard X-ray transients and classification may be premature. The combination of fast rise time, soft power-law spectrum with no high-energy cut off, lack of flickering, and highly variable light curve is not typical of the black hole candidates observed with BATSE (Paciesas *et al.* 1995). Superluminal radio emission has been observed in only one other galactic source, GRS 1915+105 (Mirabel & Rodriguez 1994) which previously had been recognized as unusual among X-ray transients

(Harmon *et al.* 1994). Except for its slow rise, the latter source strongly resembles GRO J1655-40 in hard X rays. More careful inter-comparison of these two sources may be useful in understanding their nature.

References

- Bailyn, C., Jogee, S. & Orosz, J. 1994, IAU Circ. No. 6050
Bailyn, C. *et al.* 1995, Nat (in press)
Campbell-Wilson, D. & Hunstead, R. 1994a, IAU Circ. No. 6052
Campbell-Wilson, D. & Hunstead, R. 1994b, IAU Circ. No. 6055
Crar, D. *et al.* 1995, in preparation
Della Valle, M. 1994, IAU Circ. No. 6052
Harmon, B.A. *et al.* 1994, In *The Second Compton Symposium*, C.E. Fichtel, N. Gehrels & J.P. Norris (Eds), AIP Conf. Proc. 304, p. 210
Harmon, B.A. *et al.* 1995, Nat (in press)
Hjellming, R.M. 1994a, IAU Circ. No. 6055
Hjellming, R.M. 1994b, IAU Circ. No. 6060
Hjellming, R.M. & Rupen, M. 1994a, IAU Circ. No. 6073
Hjellming, R.M. & Rupen, M. 1994b, IAU Circ. No. 6077
Hjellming, R.M. & Rupen, M. 1994c, IAU Circ. No. 6107
Hjellming, R.M. & Rupen, M. 1994d, IAU Circ. No. 6086
Hjellming, R.M. & Rupen, M. 1995, Nat (in press)
Hunstead, R. *et al.* 1994, IAU Circ. No. 6062
Hunstead, R. *et al.* 1995, these proceedings
Kroeger, R.A. *et al.* 1994, IAU Circ. No. 6051
McKay, D. & Kesteven, M. 1994, IAU Circ. No. 6062
Mirabel, I.F. & Rodriguez, L.F. 1994, Nat 371, 46
Paciesas, W.S. *et al.* 1994, IAU Circ. No. 6075
Paciesas, W.S. *et al.* 1995, In *The Gamma-Ray Sky with COMPTON/GRO and SIGMA*, M. Signore, P. Salati & G. Vedrenne (Eds), Kluwer Academic Publishers, Dordrecht, in press
Reynolds, J. & Jauncey, D. 1994, IAU Circ. No. 6063
Sunyaev, R.A. *et al.* 1991, SvAL 17, 409
Tingay, S.J. *et al.* 1995, Nat 374, 141
Wilson, C.A. *et al.* 1994, IAU Circ. No. 6056
Zhang, S.N. *et al.* 1993, Nat 366, 245
Zhang, S.N. *et al.* 1994a, IAU Circ. No. 6046
Zhang, S.N. *et al.* 1994b, IAU Circ. No. 6101
Zhang, S.N. *et al.* 1994c, IAU Circ. No. 6106

BATSE Observations of GRS 1915+105 and GRO J1655-40

W. S. PACIESAS^{a,b}, K. J. DEAL^{a,b}, B. A. HARMON^b, C. A. WILSON^b,
S. N. ZHANG^{b,c}, AND G. J. FISHMAN^b

^a *University of Alabama in Huntsville, AL 35899 USA*

^b *NASA/Marshall Space Flight Center
Huntsville, AL 35812 USA*

^c *Universities Space Research Association
Huntsville, AL 35806 USA*

INTRODUCTION

The X-ray transients GRS 1915+105 and GRO J1655-40 are the only galactic sources so far found to have superluminally expanding radio jets. We compare and contrast CGRO/BATSE hard X-ray observations with the radio behavior of these two sources in an attempt to determine whether they constitute a distinct sub-class of X-ray transients.

GRS 1915+105 was discovered by WATCH/GRANAT¹ in August 1992 but subsequent analysis of BATSE data² showed it to be present as early as May 1992. Continued monitoring^{2,3} showed that the outburst, which reached a typical (but highly variable) intensity of ~ 300 mCrab, lasted for more than 400 days until late July 1993, at which point the typical intensity dropped by at least a factor of 6. Sporadic later monitoring showed flaring activity below 20 keV in March and September 1994.³ GRS 1915+105 was identified with a variable radio⁴ and infrared^{5,6} source, but no optical counterpart has been found, probably due to strong interstellar absorption.^{7,8} VLA monitoring of the radio counterpart revealed a strong outburst in March/April 1994 which involved the ejection of a pair of bright condensations with large proper motion.⁹ At the distance of 12 kpc derived from H I absorption,⁸ the apparent velocity of the faster of these was superluminal. The inferred actual velocity of the jets was $0.92 \pm 0.08c$.

GRO J1655-40 (designated X-Ray Nova Scorpii 1994) was discovered by BATSE¹⁰ in late July 1994. Continued hard X-ray monitoring showed a rather variable light curve with no clear trend during the first outburst, which lasted ~ 18 days. Two later outbursts were observed,^{11,12} one in September lasting ~ 12 days, and another beginning in early November and still in progress as of this meeting. Identification of the optical counterpart^{13,14} led to the discovery of strong, variable radio emission¹⁵⁻¹⁷ from GRO J1655-40. The distance estimate from H I observations¹⁸ is 3.5 kpc. VLBI and VLA observations of this source showed large proper motion ejection at apparently superluminal velocities.¹⁹⁻²¹ Weaker radio outbursts were associated with the September and December X-ray outbursts.²²⁻²⁴ The radio observations and the X-ray/radio correlations are discussed in more detail elsewhere.²⁵⁻²⁷

OBSERVATIONS

The Earth occultation technique enables BATSE to function effectively as an all-sky monitor between 20 keV to roughly 1 MeV.²⁸ Routine daily operations include occultation measurements of a catalog of known or suspected sources as well as a search, albeit less sensitive, of the data for new sources not included in the catalog. The standard analysis, or alternatives, may be performed on the archival data to measure previously unrecognized sources. This enabled us retroactively to detect emission from GRS 1915+105 for several months prior to its discovery.

We have attempted to quantify certain systematic errors in the BATSE occultation analysis by studying the measured deviations from zero flux in blank-sky regions. In general, we find a larger spread of the data than expected from statistics alone, the typical measured standard deviation being 20–30% greater. However, for sources in the Aquila region, which includes GRS 1915+105, the excess spread is even larger. When we performed such an analysis for the location of GRS 1915+105 prior to TJD 8730, which is consistent with zero average flux, the measured standard deviation was larger than the statistical prediction by a factor of 2.183.

The BATSE long-term intensity history of GRS 1915+105 is shown in Fig. 1, where we have increased the error bars by 2.183 in order to account for the systematic deviations. The hard X-ray emission from the source is confined primarily to two episodes: the original outburst lasting about 430 days from May 1992 to July 1993 and a secondary outburst lasting about 110 days from December 1993 to March 1994. Although quite variable on the ten-day timescale shown, the typical flux during both outbursts is similar: ~ 0.06 to $0.08 \text{ ph cm}^{-2} \text{ s}^{-1}$ (20–100 keV), roughly 200–250 mCrab. There is also indication of persistent but variable lower-level emission of ~ 30 mCrab between and after the main outbursts. In particular, the flare beginning around TJD 9610 was also observed at lower energies.^{3,29}

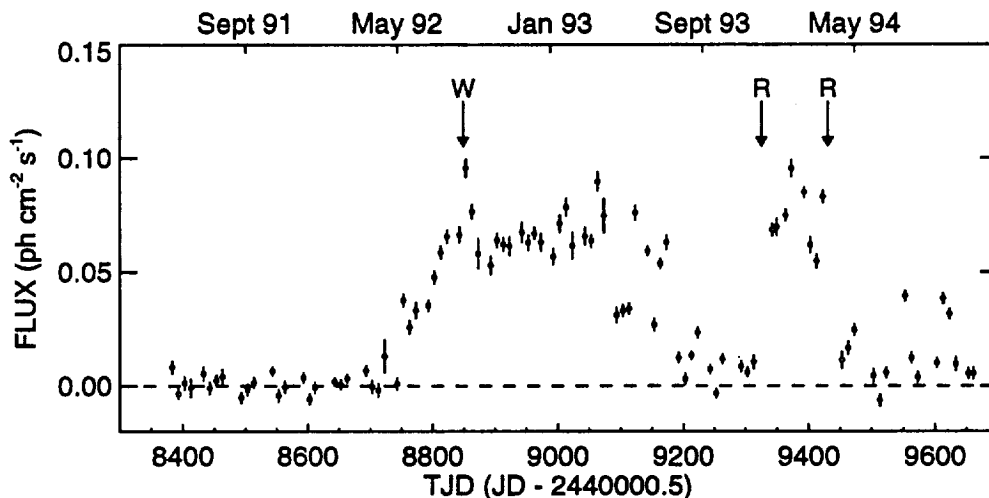


FIGURE 1. Intensity history of GRS 1915+105 in the energy range 20–100 keV. The points are averages of 10 days. The arrow marked W indicates the time of the WATCH discovery.⁶ The arrows marked R indicate the times of radio flares.

Figure 2 shows the BATSE-determined intensity history of GRO J1655–40. The errors shown are statistical only, since we have not yet investigated the systematic fluctuations for this source. However, our previous experience indicates that

systematic deviations in the Scorpius region are no greater, and probably much less, than those in Aquila. For this source, we identify three outburst episodes: the initial one of ~ 17 days which ended in mid-August, a slightly weaker one lasting ~ 10 days in September, and a longer, more intense one, beginning in early November and still in progress at the time of this symposium.^a The typical flux during outburst is ~ 4 times that of GRS 1915+105, implying that the latter is ~ 3 times more luminous in hard X-rays than GRO J1655-40 if the distance estimates are correct.

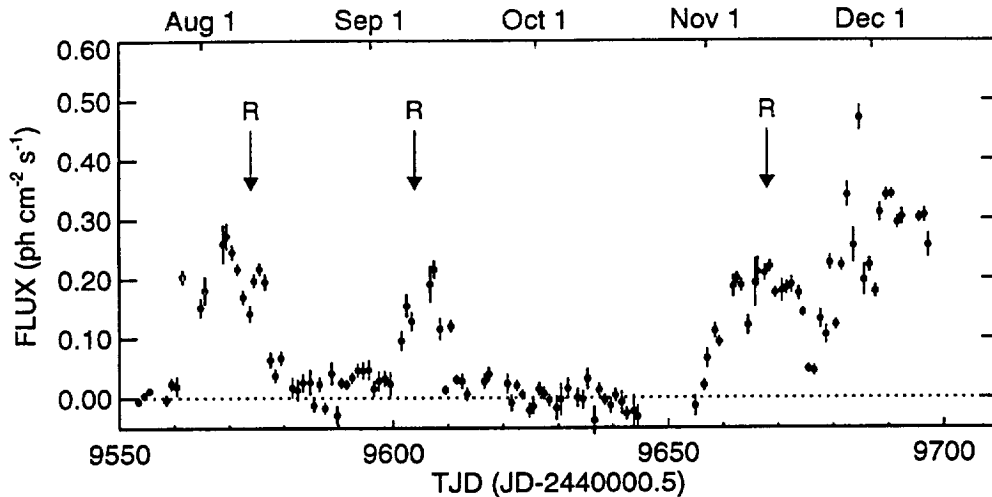


FIGURE 2. The intensity history of GRO J1655-40 in the energy range 20-100 keV. The points are averages over 1 day. Arrows marked R indicate the times of radio flares.

DISCUSSION

The radio counterpart of GRS 1915+105 was discovered in December 1992,⁴ and thus radio coverage during the first hard X-ray outburst was incomplete. The two major radio flares of which we are aware occurred during the second hard X-ray outburst (indicated by arrows in Fig. 1). The first of these, in December 1993,³⁰ occurred near the hard X-ray rise and the second, including the VLA ejection event in March 1994,⁹ coincides approximately with the hard X-ray decline. Unfortunately, the BATSE occultation analysis is affected by interference from other sources during the latter interval, and we cannot determine the time of the hard X-ray decrease more precisely without further study.

In GRO J1655-40, the radio flares are progressively less intense and their correspondence with hard X-ray outbursts is quasi-consistent, i.e., the first radio flare¹⁷ coincides with the end of the first hard X-ray outburst, whereas the second radio flare^{22,23} peaks around the middle of the second hard X-ray outburst and the third radio flare²⁴ peaks during the early part of the third outburst (an alternative interpretation is that the more intense hard X-ray emission after \sim TJD 9680 is a fourth flare, in which case the third radio and X-ray flares coincide well while the inferred fourth radio flare may have been too weak to detect).

These preliminary results suggest some kind of correspondence between radio and hard X-ray activity in both sources; however, there is no simple one-to-one

^a Subsequent BATSE data shows the outburst ending around TJD 9705 (19 Dec 1994).

relationship and the nature of the correlation is not consistent. We conclude that the radio and hard X-ray fluxes are affected in different ways by some more fundamental factor such as the local accretion rate in the inner disk.

It is interesting to consider whether superluminal radio jets are associated with a distinct subclass of X-ray novae. Although there are obvious differences in overall duration, the hard X-ray light curves of GRS 1915+105 and GRO J1655-40 have more in common with each other than with the "typical" X-ray nova. The latter may generally be described as having a smooth (on timescales of several days) decaying trend, usually exponential, with a weaker re-flare occurring a few months after the initial maximum. In contrast, Figs. 1 and 2 show strong variability within each outburst, with no clear maximum and no decaying trend, and the later outbursts are at least as strong, or stronger, than the first. Additionally, both sources have steeper hard X-ray spectra than other X-ray novae^{2,25} and an unusually small difference in optical luminosity between outburst and quiescence was found for GRO J1655-40.¹⁴ If this separate classification is supported by further studies, an obvious question to consider is whether the distinction is fundamental, such as a difference in the mass or nature of the compact object, or an accident of our observational perspective, as in the unified model for active galactic nuclei.

REFERENCES

1. CASTRO-TIRADO, A. *et al.* 1994. *Ap. J. Suppl. Ser.* **92**: 469-472.
2. HARMON, B. A. *et al.* 1994. *In* AIP Conf. Proc. No. 304. C. E. Fichtel, N. Gehrels & J. P. Norris, Eds.: 210-219. Am. Inst. Physics. New York, New York.
3. SAZONOV, S. YU. *et al.* 1994. *Astronomy Letters* **20**: 787-791.
4. MIRABEL, I. F. *et al.* 1993. *IAU Circ. No.* 5773.
5. MIRABEL, I. F. *et al.* 1993. *IAU Circ. No.* 5830.
6. CASTRO-TIRADO, A., S. A. BRANDT & N. LUND. 1993. *IAU Circ. No.* 5830.
7. GREINER, J. *et al.* 1994. *In* AIP Conf. Proc. No. 304. C. E. Fichtel, N. Gehrels & J. P. Norris, Eds.: 260-264. Am. Inst. Physics. New York, New York.
8. MIRABEL, I. F. *et al.* 1994. *Astron. Astrophys.* **282**: L17-L20.
9. MIRABEL, I. F. & L. F. RODRIGUEZ. 1994. *Nature* **371**: 46-48.
10. ZHANG, S. N. *et al.* 1994. *IAU Circ. No.* 6046.
11. PACIESAS, W. S. *et al.* 1994. *IAU Circ. No.* 6075.
12. ZHANG, S. N. *et al.* 1994. *IAU Circ. No.* 6101.
13. BAILYN, C., S. JOGEE & J. OROSZ. 1994. *IAU Circ. No.* 6050.
14. BAILYN, C. D. *et al.* 1995. *Nature*, in press.
15. CAMPBELL-WILSON, D. & R. HUNSTEAD. 1994. *IAU Circ. No.* 6052.
16. HJELLMING, R. M. 1994. *IAU Circ. No.* 6055.
17. CAMPBELL-WILSON, D. & R. HUNSTEAD. 1994. *IAU Circ. No.* 6055.
18. MCKAY, D. & M. KESTEVEN. 1994. *IAU Circ. No.* 6062.
19. REYNOLDS, J. & D. JAUNCEY. 1994. *IAU Circ. No.* 6063.
20. HJELLMING, R. M. & M. RUPEN. 1994. *IAU Circ. No.* 6073.
21. HJELLMING, R. M. & M. RUPEN. 1994. *IAU Circ. No.* 6086.
22. HJELLMING, R. M. & M. RUPEN. 1994. *IAU Circ. No.* 6077.
23. CAMPBELL-WILSON, D., D. J. MCKAY & J. E. LOVELL. 1994. *IAU Circ. No.* 6078.
24. HJELLMING, R. M. & M. RUPEN. 1994. *IAU Circ. No.* 6107.
25. HARMON, B. A. *et al.* 1995. *Nature*, in press.
26. TINGAY, S. J. *et al.* 1995. *Nature*, **374**: 141-143.
27. HJELLMING, R. M. & M. RUPEN. 1995. *Nature*, submitted.
28. HARMON, B. A. *et al.* 1992. *In* The Compton Observatory Science Workshop. C. R. Shrader, N. Gehrels & B. Dennis, Eds.: 69-75. NASA CP-3137.
29. ALEXANDROVICH, N., K. BOROZDIN & R. SUNYAEV. 1994. *IAU Circ. No.* 6080.
30. RODRIGUEZ, L. F. & I. F. MIRABEL 1993. *IAU Circ. No.* 5900.

THE CONTINUUM SPECTRAL CHARACTERISTICS OF GAMMA-RAY BURSTS OBSERVED BY BATSE

GEOFFREY N. PENDLETON, WILLIAM S. PACIESAS, MICHAEL S. BRIGGS,
ROBERT S. MALLOZZI, AND TOM M. KOSHUT
Department of Physics, University of Alabama in Huntsville, Huntsville, AL 35899

GERALD J. FISHMAN, CHARLES A. MEEGAN, ROBERT B. WILSON, AND ALAN B. HARMON
NASA/Marshall Space Flight Center, Huntsville, AL 35812

AND

CHRYSSA KOUVELIOTOU¹

Universities Space Research Association

Received 1993 August 30; accepted 1994 February 10

ABSTRACT

Distributions of the continuum spectral characteristics of 260 bursts in the first BATSE catalog are presented. The data are derived from flux ratios calculated from the BATSE Large Area Detector (LAD) four-channel discriminator data. The data are converted from counts to photons using a direct spectral inversion technique to remove the effects of atmospheric scattering and the energy dependence of the detector angular response. Although there are intriguing clusterings of bursts in the spectral hardness ratio distributions, no evidence for the presence of distinct burst classes based on spectral hardness ratios alone is found. All subsets of bursts selected for their spectral characteristics in this analysis exhibit spatial distributions consistent with isotropy. The spectral diversity of the burst population appears to be caused largely by the highly variable nature of the burst production mechanisms themselves.

Subject heading: gamma rays: bursts

1. INTRODUCTION

This analysis of BATSE data (Fishman et al. 1989a, b) presents the coarse spectral characteristics of an ensemble of 260 gamma-ray bursts (GRBs) observed by BATSE from 1991 April 23 to 1992 March 5. Previous observations of GRBs (e.g., Higdon et al. 1990) have shown that they exhibit extremely hard spectra that are in general softer at higher energies than they are at lower energies (Wheaton et al. 1973; Cline et al. 1973). They can be characterized in general by a quasi-exponential component at lower energies and in some cases a power-law component at higher energies. Many bursts appear to be consistent with power-law spectra to 100 MeV (Matz et al. 1985; Kwok et al. 1993). Evidence for striking spectral diversity is present in the earlier measurements (Mazets et al. 1981) as well as in more recent analyses (Band et al. 1993). The data presented here are in agreement with the previously observed spectral behavior and provide an overview of the entire range of continuum spectra that bursts exhibit in the energy range from 25 to 2000 keV. The LAD data of unprecedented sensitivity are available for all the bursts in the viewing period specified above and provide one of the largest samples of burst spectral data from a single instrument to date.

2. ANALYSIS

The analysis primarily employed DISCSC (Summed LAD discriminator counts) and PREB (preburst) (Fishman et al. 1989) data for the bursts. The DISCSC data consist of four broad channels corresponding to the energy ranges 20–50 keV, 50–100 keV, 100–300 keV, and $E > 300$ keV for the BATSE LAD's. The data are summed over all detectors that measured

the burst flux at a rate greater than or equal to 5.5σ above background in the energy range 50–300 keV at the time of the burst trigger (Meegan 1991). They have 64 ms time resolution covering the time interval from the burst trigger to 240 s after the burst trigger. The PREB data have the same energy binning and time resolution as the DISCSC data. They are collected for each individual LAD in a sliding buffer that covers the interval from -2.0 s to the burst trigger time. For the purposes of this analysis the PREB data are summed over the detectors included in the DISCSC data. DISCLA (LAD discriminator) data with 1.024 s resolution were used for calculating background. If a burst had emission outside the -2 to 240 s interval covered by the combined PREB and DISCSC data, then background-subtracted DISCLA data were added to complete the fluence calculation.

Background subtraction was performed using a quadratic fit to the count rates in each channel of each detector derived from appropriate 1.024 s resolution background intervals around the burst. Figure 1 shows all the elements employed in the background subtraction for trigger 160 (1B 910507) in each discriminator channel. The reduced χ^2 's for the background fit averaged ~ 1.13 .

Two spectra were selected for each burst in this analysis: a 64 ms peak rate spectrum and a total fluence spectrum. The 64 ms peak spectrum was selected by choosing the interval with the largest count rate in discriminator channels 2 and 3 (50–300 keV) from the 64 ms data. The total fluence spectrum was produced by summing all the flux in the burst interval.

The counts data were converted to photons by applying two iterations of a direct matrix inversion technique. For this procedure detector response matrices (DRMs) (Pendleton et al. 1989) that included atmospheric scattering corrections (Pendleton et al. 1992) were generated for each burst. They

¹ Postal address: NASA Marshall Space Flight Center, Huntsville, AL 35812.

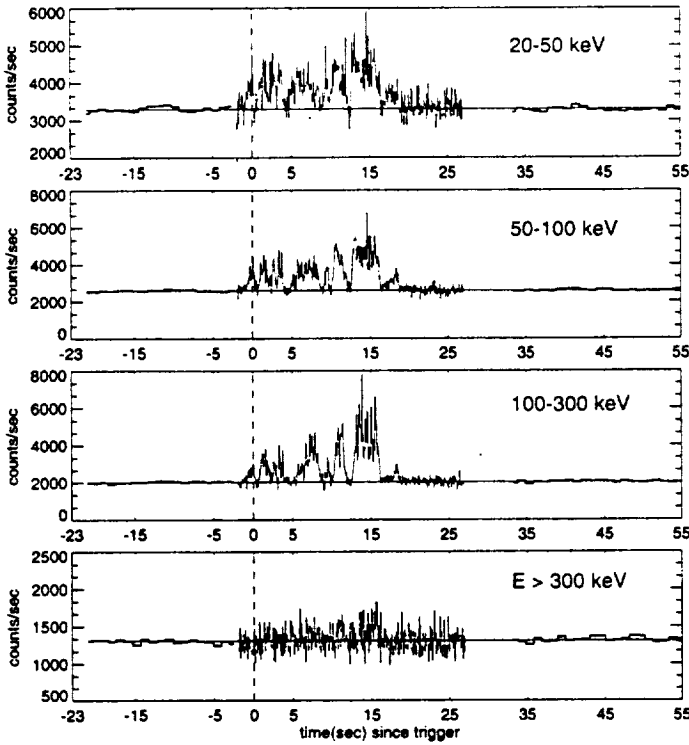


FIG. 1.—Histograms showing the source and background counts for channel 1: 20–50 keV, channel 2: 50–100 keV, channel 3: 100–300 keV, and channel 4: $E > 300$ keV for trigger 160 (1B 910507). The thin histogram at the center of each plot shows the source plus background data in each channel summed over detectors 1 and 3 on a 64 ms timescale. The thick histograms on either side show the 1.024 s time resolution data used for the quadratic background fit. The thin line spanning the entire interval shown is the quadratic background that is subtracted from the counts in the burst interval. The vertical dashed lines in the plots show the burst trigger time.

were binned with the four-channel energy resolution of the counts data. This broad energy binning of the DRM's necessitated the inclusion of some estimate of the spectral index of the incident photon spectrum across each bin. For example, 50 keV photons contribute to the four channel count spectra very differently from 100 keV photons. Having some estimate of the ratio of 50 to 100 keV photons in the incident spectra is important in order to convert the counts data to photon spectra accurately.

In the first iteration the matrices were generated with an assumed power-law index of -0.5 across the first three discriminator bins and an index of -1.1 in the $E > 300$ keV bin. Then, for each burst, the DRM was mathematically inverted. This inverted matrix then represented the quantitative conversion of observed counts to incident photons. The matrix multiplication of the four-element vector of counts data with the inverse DRM produced a four-element vector of photon data. The results of this first application of the matrix inversion procedure to the ensemble of burst data produced a wide variety of burst spectra. Many of these spectra had spectral indices that differed significantly from those applied across the matrix bins in the first iteration of the DRM calculations.

Assuming a spectral index across the matrix bin that more accurately represents the continuum spectrum being studied increases the accuracy of the spectral inversion technique. To obtain a first-order estimate of the spectral indices for the burst continuum spectra, a quadratic was fitted to the four-photon

data points expressed in $\log(\text{photons cm}^{-2} \text{ keV}^{-1})$ versus the logarithmic bin centers expressed in $\log(\text{keV})$. This is quantitatively equivalent to finding the best-fit parabola to the data on a log-log plot. This fit provides a first-order estimate of the amplitude and spectral index of the continuum for each data point.

The DRMs were then recalculated, weighting the spectra across the photon input bins using the slopes found with the quadratic fit in order to more accurately represent each burst continuum spectrum. These matrices were then inverted and applied to the counts data. In some cases the resulting photon spectra differ significantly from those of the first iteration in channel four ($E > 300$ keV). The other photon data remained quite stable between iterations.

The data presented here are expressed in the form of effective power-law spectral indices calculated for each pair of adjacent bins in the photon spectrum. The formula relating the ratio of photons observed in bins i and $i + 1$ to an effective power-law index, α is

$$\frac{\int_{E_i}^{E_{i+1}} E^\alpha dE}{\int_{E_{i-1}}^{E_i} E^\alpha dE} = \frac{P_i}{P_{i+1}}, \quad (1)$$

where P_i is the photon flux observed in the i th channel and P_{i+1} is flux in the $i + 1$ th channel.

This equation was evaluated numerically over a range of α 's for the three ratios of adjacent channels. The 1σ error ranges on the photon data ratios were transformed via this equation to 1σ error ranges on the effective spectral indices.

This technique was applied to Crab flux obtained with BATSE occultation software (Harmon et al. 1992) using DISCLA data to determine its accuracy. This analysis revealed that the LAD discriminator overflow bin (channel 4, $E > 300$ keV) was effectively represented by a detector response matrix element that extends from 300 to 6500 keV. It must be remembered, however, that there is no spectral information in this energy range in the DISCLA data. The channel 4 data can be used to determine if the higher energy flux is consistent with a particular simple spectral form but more detailed information must be obtained from data types with higher energy resolution.

There were bursts out of the set of 260 that did not have measurable flux in all channels for either the peak rate or total fluence. In the cases where only upper limits were available no spectral index was calculated. All 260 bursts had measurable flux in channels 2 and 3 as a consequence of the trigger criterion. However, some bursts did not have measurable flux in channels 1 and 4. Table 1 presents the totals of the bursts based on the significance of the observed rates in channels 1 and 4. The numbers in the channel 1 columns apply to bursts that have measurable flux in channel 1. Conversely, the No. Channel 1 columns refer to bursts without significant channel 1 flux. The rows are defined similarly for channel 4 flux. The totals are presented separately for the peak fluxes and total fluences.

3. PEAK FLUX AND FLUENCE SPECTRAL DISTRIBUTIONS

Effective power-law indices characterizing the peak flux and fluence continuum spectra of the bursts are presented as scatter plots and as histograms in Figures 2–9. Some numerical information is presented in tabular form. Figures 2a–4d show scatter plots of the spectral indices for the entire ensemble of bursts. These spectral indices are plotted with the higher

TABLE 1
TOTALS OF CHANNEL 1 AND 4 FLUX AND FLUENCE CASES
A. FLUX CASE
B. FLUENCE CASE

Peak Flux	Channel 1	No Channel 1	Fluence	Channel 1	No Channel 1
Channel 4	169	23	Channel 4	209	4
No Channel 4	56	12	No Channel 4	47	0

energy indices on the vertical axis and the lower energy indices on the horizontal axis. Plotting these indices simultaneously gives an estimate of the curvature of the spectra over the total energy range displayed in the scatter plot. Also shown on these plots is a dotted line representing power-law spectra. Points below this line correspond to spectra that have a concave downward curvature on log-log plots of photons/keV versus photon energy. These are spectra that are softer at higher energies. Points above the power-law line correspond to spectra that are concave up on log-log plots (i.e., spectra that are harder at higher energies).

The upper left-hand plots (2a, 3a, and 4a) of these figures show the spectral indices of the 64 ms peak fluxes for the bursts. The spectral index axis limits for these plots were picked to focus on the distribution of the vast majority of

bursts. (The histogram plots have larger ranges to show the extremes of the spectral index distributions.) Each square on these plots represents an individual burst. The error bars are omitted from these plots for clarity.

The effective spectral indices for Crab occultation data summed over 1 day for each of the 8 LAD detectors are shown as diamonds on these plots. The size of the diamonds show the errors for each point. These spectral indices are in reasonable agreement with previous measurements (Jung et al. 1989) of the steady Crab flux in the same energy range. Comparisons have been made between the burst spectral indices presented here and those obtained using the spectroscopy detector data (Band et al. 1993). There is agreement between the LAD and SPEC detector results when similar time and energy intervals are compared. In particular, Band's high-energy spectral indices

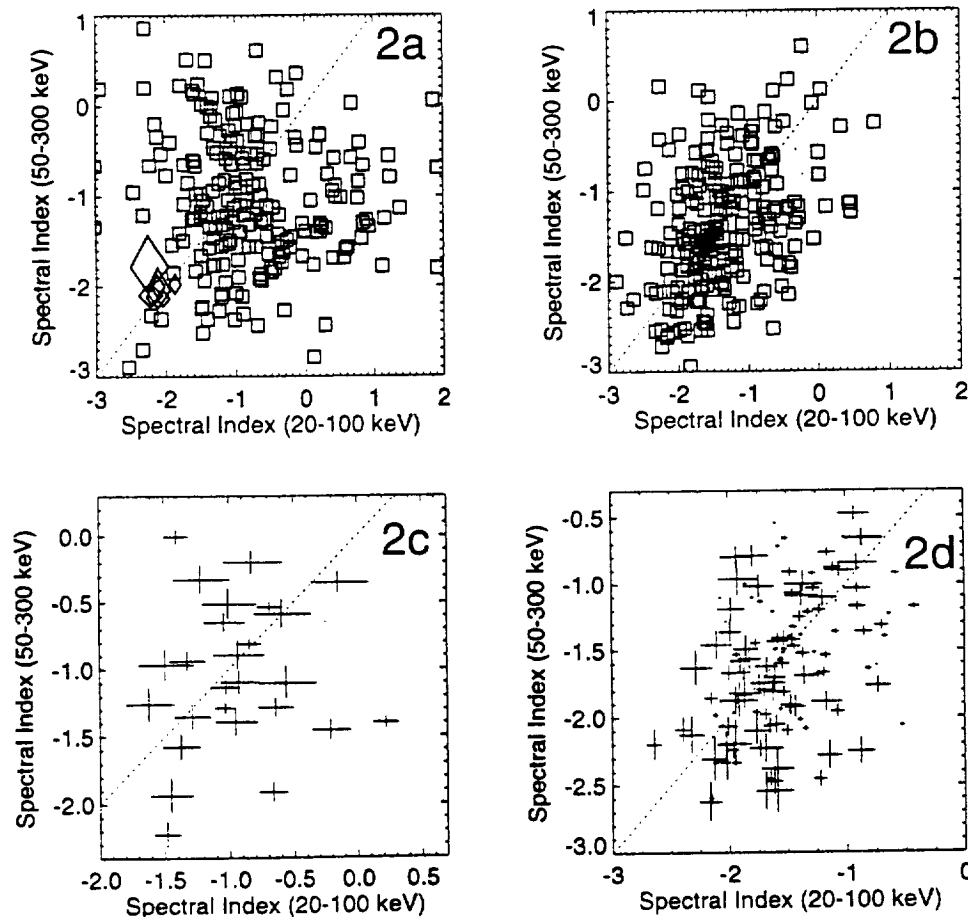


FIG. 2.—(a–d) These figures show scatter plots of power spectral indices for the 20–100 keV range vs. the 50–300 keV range for the gamma-ray bursts. The direct crab flux spectral indices are represented by diamonds on these plots. (a) 64 ms peak rate data. (b) Spectral indices of the total fluence. (c) Subset of the 64 ms peak flux data points where the errors in the spectral indices are less than 0.5 in both the 20–100 keV and 50–300 keV range. (d) Subset of the total fluence spectral indices with the same error constraints as (c).

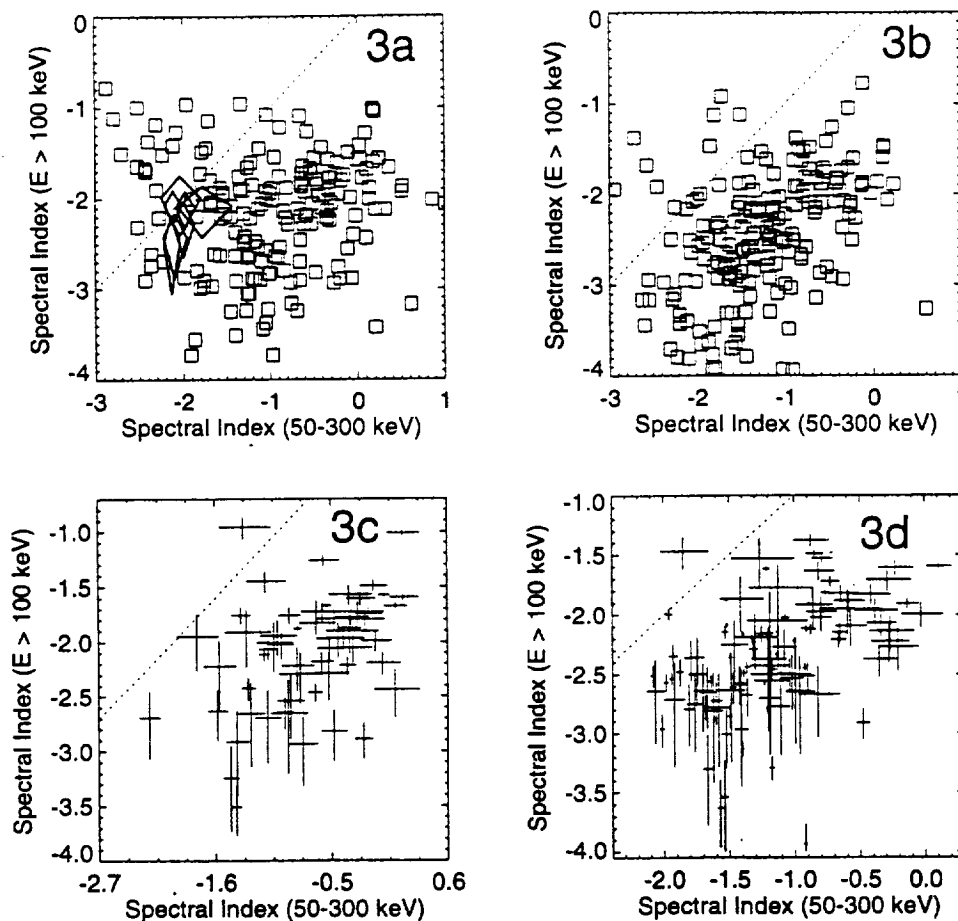


FIG. 3.—(a–d) The data in these figures are presented in the same format as in Fig. 2a–2d except that here the indices in the 50–300 keV range are compared to the indices for the energy $E > 100$ keV. The error constraints for (c) and (d) are data points with indices less than 0.5 in the 50–300 keV range and 1.0 in the $E > 100$ keV range.

for burst fluence measurements agree with those presented here for bursts 1B 910421, 1B 910629, and 1B 911118.

The lower left-hand plots (Figs. 2c, 3c, and 4c) are the subset of the data shown in the upper right-hand plots that are well determined and reveal some of the underlying structure of the spectral index distribution.

The right-hand plots mimic the left-hand plots in format. They show the spectral indices for the total fluence of the bursts. The integration times for these spectra range from 64 ms to hundreds of seconds. The longer integration times result in smaller errors as can be seen in the lower right-hand plots (Figs. 2d, 3d, and 4d).

The broad distribution of burst spectral states is evident in this data. One interesting feature of some of the 20–300 keV spectra shown in Figure 2 scatter plots is that they exhibit hardening of the spectra with energy up to 300 keV. Figure 2d shows burst fluences that are many sigma above the power-law line indicating concave up spectra. Spectra like these have been observed before (Mazets et al. 1981; Murakami et al. 1988). These kind of spectra may indicate the presence of more than one spectral component contributing to the spectra simultaneously. No significant evidence for this type of spectral behavior is evident in any of the other energy ranges studied here.

The higher energy range data shown in the Figure 3 plots show general concave down behavior above 50 keV. There is

quite a range of spectral indices but the power-law line seems to be an upper bound for these spectra. In fact, most of the bursts show at least a 0.5 spectral index softening between the 50–300 keV range and the $E > 100$ keV range.

The total energy range ($E > 20$ keV) plots of Figure 4 also show spectra that in general become softer with increasing energy. In both the high-energy and total energy range plots there are bursts consistent with power-law spectra. However the plots showing spectra with smaller error bars show no significant number of bursts exhibiting concave up behavior over these energy ranges.

The spectral diversity of the burst population prompts the question of whether two or more subclasses of bursts can be resolved by studying the distribution of their spectral continuum properties. In fact, the original impetus for this research was to identify spectrally distinct subclasses of bursts that exhibited significantly different spatial distributions. For example, if a set of galactic disk objects observed well out into the disk were contributing bursts of one spectral type and cosmological sources were contributing bursts of another spectral type, then the spatial distributions of these two types of bursts would be different. No evidence for this type of behavior is seen in these data.

The scatter plots of the burst spectral characteristics show a complex distribution of GRB spectra that might possibly be

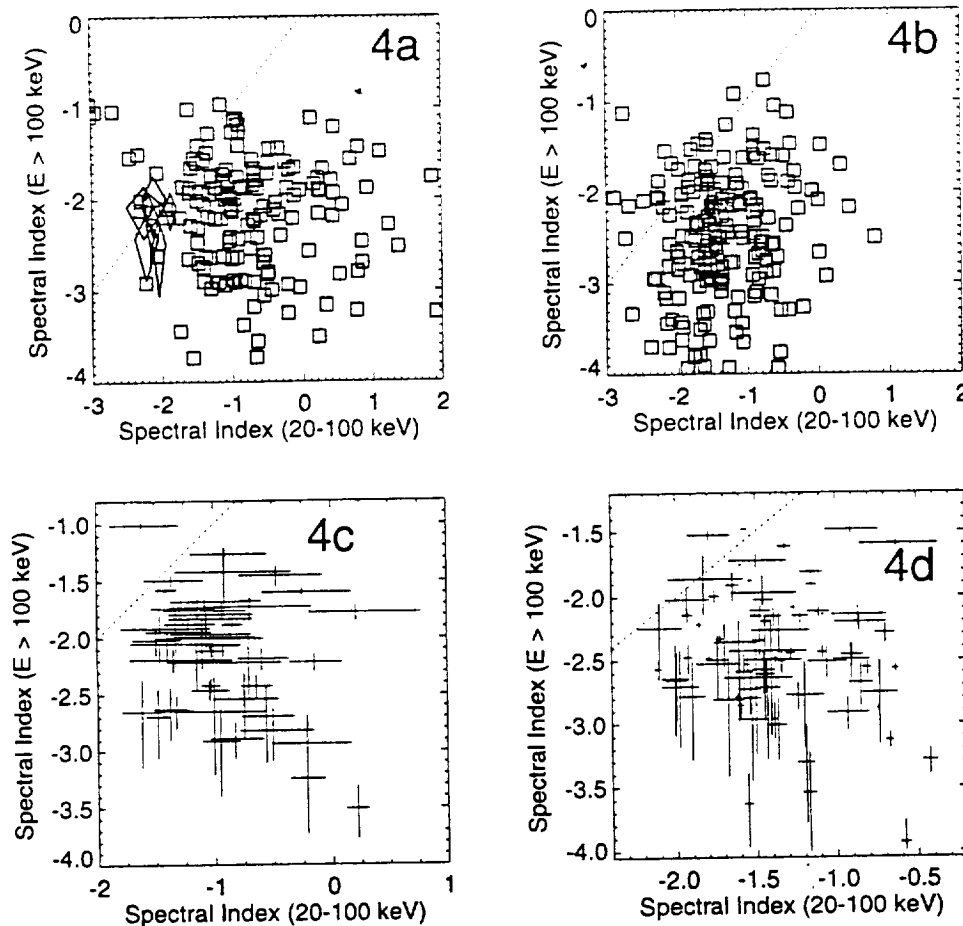


FIG. 4.—(a–d) The data here are presented in the same format as in Fig. 2a–2d except that here the indices in the 20–100 keV range are compared to the indices for the energy range $E > 100$ keV. The error constraints for (c) and (d) are data points with indices less than 0.5 in the 20–100 keV range and 1.0 in the $E > 100$ keV range.

resolved into a significantly multimodal distribution at some future time when enough bursts have been measured. Already a bimodal duration distribution has been identified in the BATSE burst data (Kouveliotou et al. 1993). The bursts in the short duration class show significantly harder fluences on average than the longer duration bursts. Figure 5 shows the

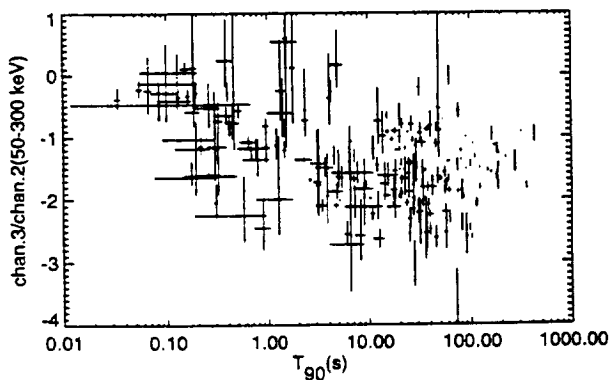


FIG. 5.—The spectral indices of the bursts total fluences in the energy range 50–300 keV are plotted vs. duration (T_{90}). Here T_{90} is defined (see Kouveliotou et al. 1993) as the length of the interval containing the middle 90% of the burst fluence.

spectral index of the total fluence in the 50–300 keV range versus burst duration. This plot is quite similar to Figure 4 of Kouveliotou et al. (1993). The Spearman rank-order analysis shows a correlation between hardness and duration with a chance fluctuation probability of 2×10^{-7} . However the range of spectral behaviors exhibited by both the short- and long-duration bursts is quite broad, and they cannot be confidently isolated from each other using the data set presented here. This conclusion is also reached by Kouveliotou et al. (1993).

Spatial distributions of possible spectral subsets of bursts were studied and found to be consistent with isotropy. Figures 2b and 2d show some clustering of burst fluences about a spectral index of approximately -1.7 in the 50–300 keV and 20–100 keV ranges. There are some other bursts loosely scattered around -1.0 on these plots as well. The bursts were split into two sets centered about these spectral indices; however the spatial distributions of these two sets are consistent with isotropy. Table 2 shows dipole $\langle \cos \theta \rangle$ and quadrupole $\langle \sin^2 b - \frac{1}{3} \rangle$ moments calculated in galactic coordinates of spectral subsets of bursts. Also shown in the table are the values expected for a uniform distribution viewed through the BATSE sky map. The inequalities in the table show the dividing lines between the spectral subsets. There are also bursts which show a dearth of emission above 300 keV. These bursts, without significant flux/fluence in channel 4 (see Table 1), are consistent with isotropy as well.

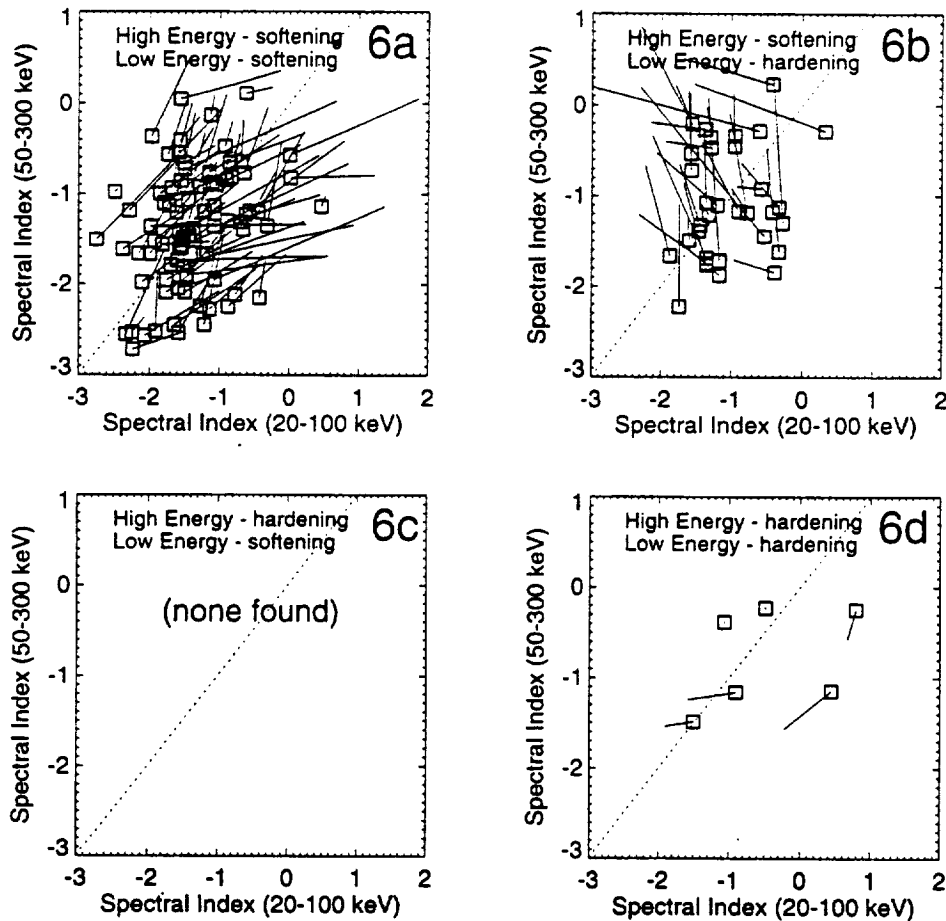


FIG. 6.—(a–d) These figures show scatter plots of the changes in spectral power indices between the 64 ms peak fluxes and the total fluences for the 20–100 keV range vs. the 50–300 keV ranges. The squares in these plots are the total fluence points. The lines extending from these boxes end at the 64 ms peak spectra points. These lines show the direction of the spectral changes between peak flux and total fluence of the power-law indices for the bursts. The data are separated into four plots to aid in visual interpretation. The upper left-hand plot shows softening of both the higher energy and lower energy total fluence spectral indices with respect to the peak flux indices. The upper right hand plot shows softening of the higher energy indices and hardening of the lower energy indices. The lower left-hand plot shows hardening of the higher energy indices and softening of the lower energy indices. The lower right-hand plot shows hardening of both the higher energy indices and the lower energy indices.

4. CHANGES OF SPECTRAL INDICES WITHIN BURSTS

There is significant variability of the spectra within individual bursts. The changes in spectral indices for bursts between their 64 ms peak spectra and the total fluence spectra are shown in the scatter plots of Figures 6a–8d.

The spectral changes shown in the Figure 6 plots show mostly a softening of the fluence relative to the peak spectrum

in the 20–100 keV range. This softening trend occurs in an even larger fraction of the bursts in the 50–300 keV range. It is interesting to note that none of the bursts showed a hardening of the fluence with respect to the peak spectrum in the 50–300 keV range coupled with a softening in the 20–100 keV range.

These spectral index change plots show in general a tendency toward softening of the fluence spectra with respect to the peak spectra. Only a few events exhibit hardening of the

TABLE 2
SPATIAL MOMENTS OF SPECTRAL SUBSETS

Subset Constraints Uniform Distribution	$\langle \cos \theta \rangle$ of Subset –0.013	$\langle \sin^2 b - \frac{1}{3} \rangle$ of Subset –0.005
$IF_{32} > -0.71IF_{21} - 2.26$	0.016 ± 0.047	-0.037 ± 0.024
$IF_{32} < -0.71IF_{21} - 2.26$	0.017 ± 0.055	-0.016 ± 0.029
$IP_{32} > -0.27IP_{21} - 1.01$	0.052 ± 0.055	-0.038 ± 0.028
$IP_{32} < -0.27IP_{21} - 1.01$	-0.010 ± 0.047	-0.020 ± 0.025
No channel 4 peak flux	-0.001 ± 0.070	0.021 ± 0.036
No channel 4 fluence	-0.008 ± 0.068	-0.015 ± 0.035

^a IF_{32} is the fluence spectral index across channels 2 and 3.

^b IP_{32} is the peak flux spectral index across channels 2 and 3.

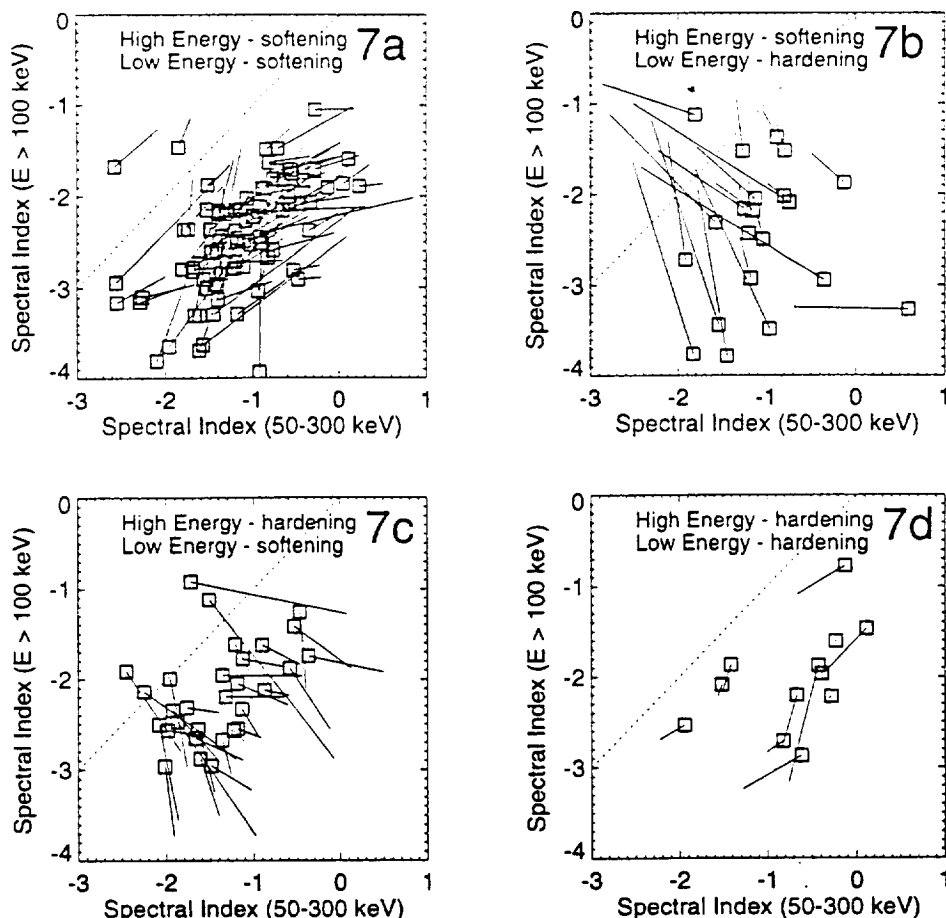


FIG. 7.—(a–d) These plots have the same format as plots Figs. 5a–5d. Here the changes in spectral indices between peak flux and total fluence are being shown for the 50–300 keV range and the $E > 300$ keV range.

fluence spectra with respect to the peak spectra (Fig. 6d, 7d, and 8d).

Figures 9a–9c compare the peak flux and fluence spectral index distributions in histogram form. Quantitative studies of these spectral index distributions have been made on appropriate sets of bursts. For each energy range bursts were selected that had measurable spectral indices in both the peak spectra and fluence spectra. Table 3 summarizes the averages of the spectral index distributions. Here column (2) shows the number of bursts in each set. Column (3) contains the average of the fluence spectra distribution in the specified energy range. Column (4) contains the same information for the 64 ms peak spectra. Column (5) contains the average of the peak spectra distribution corrected for selection effects.

There are two selection effects that impact the peak rate spectra due to the fact that there are on average ~ 10 64 ms

spectra within 1σ of the peak spectrum in the 50–300 keV range. One effect is that selecting the brightest of these spectra based on the 50–300 keV counts flux will generally result in the highest statistical fluctuations being chosen for channels 2 and 3. Since channels 1 and 4 are outside this energy range, they will not be subject to the same statistical selection effect and only values distributed about the average intensity near the peak will be chosen. However, countering this effect is the detector response characteristic that a continuum of photons spanning channel 1 will produce some counts in channel 2 as well due to the width of the detector resolution. High-energy photons that mainly contribute to channel 4 sometimes are recorded in the lower channels instead due to partial energy deposition. Hence higher rates in channels 1 and 4 imply some spill over to channels 2 and 3. Monte Carlo simulations were made to quantify the impact of these selection effects on the peak rate spectral index calculations as a function of intensity, spectral index, and number of 64 ms spectra within 1σ sigma of the peak. The results of the simulations were applied to the observed data to produce the corrected averages.

The general softening of the fluence with respect to the peak flux is evident in the Figure 9 plots and the Table 3 data, particularly in the 20–100 keV range. These results mean that the more intense portions of bursts are usually comprised of harder spectra than the less intense portions, but this does not necessarily apply to all bursts. It is also clear that the spectra

TABLE 3
SPECTRAL INDEX DISTRIBUTION AVERAGES

Energy Range (keV) (1)	Number of Bursts (2)	Fluence Average (3)	Peak Average (4)	Corrected Peak Average (5)
20–100	224	-1.41 ± 0.050	-0.73 ± 0.075	-0.71
50–300	260	-1.38 ± 0.055	-1.13 ± 0.057	-1.09
$E > 100$	164	-2.46 ± 0.069	-2.19 ± 0.058	-1.96

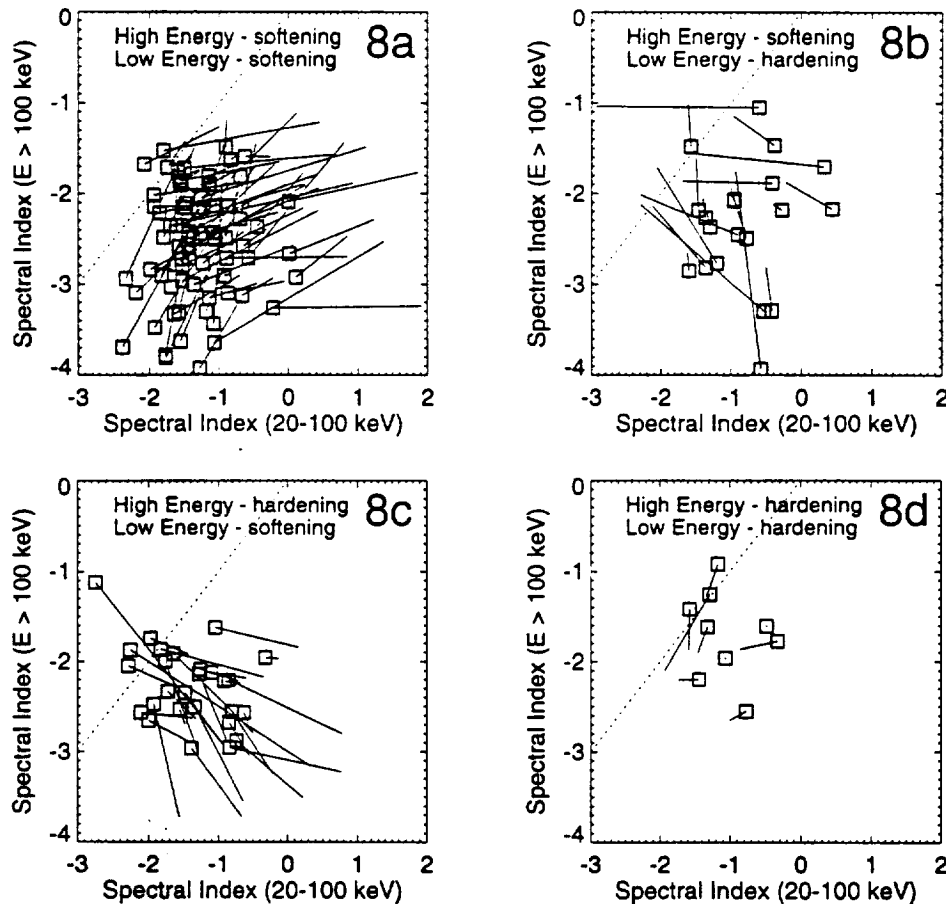


FIG. 8.—(a–d) These plots have the same format as plots in Figs. 5a–5d plots. Here the changes in spectral indices between peak flux and total fluence are being shown for the 20–100 keV range and the $E > 300$ keV range.

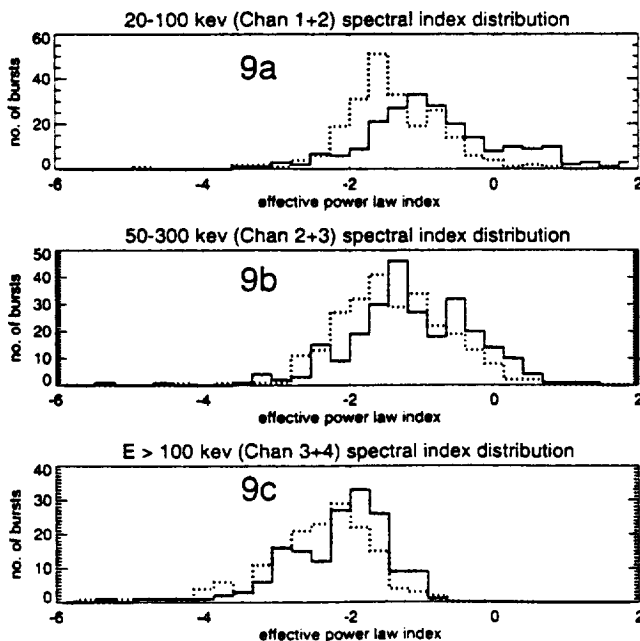


FIG. 9.—(a–d) These are histograms of the spectral indices over the three energy ranges studied here. The solid lines represent the distribution for the peak rate spectra and the dotted lines show the distribution for the total fluence spectra. (a) The spectral index distributions for the energy range 20–100 keV, (b) 50–300 keV, (c) $E > 100$ keV.

change significantly within individual bursts. These results are consistent with previous burst studies. A point that can be emphasized with this large and exhaustive burst data set is that the spectral changes between peak flux and fluence for individual bursts can span a significant portion of the spectral range of the entire burst distribution. This behavior suggests that the highly variable nature of the burst emission mechanisms may be responsible for the variety of burst spectra observed. It is likely that the bursts observed share common physical production mechanisms that happen to be highly variable.

Another qualitative observation of the 20–100 keV histograms is that the distribution of average spectral indices appears to have more clustering in it than the peak spectral index distribution. However, the distribution widths are dependent on the statistical significance of the two data sets. Simulations show that the difference in the width of the peak flux and fluence distributions is consistent with the differences in the statistical significances of these data sets.

5. SUMMARY

In general, the burst spectra are softer at higher energies than at lower energies. This is consistent with other observations (Mazets et al. 1981). Some of the spectra seem to have complex spectral structure switching from concave down to concave up over different energy ranges. Complex spectral structure has been noted in bursts before as well (Mazets et al. 1988; Mitrofanov et al. 1992). There is no evidence for clearly

independent spectral classes of objects manifesting their existence through this analysis. The spatial distributions of all subsets examined are consistent with the entire burst ensemble distribution. It seems more likely that the spectral diversity of the burst phenomenon represents the variable nature of the physical mechanisms that produce the bursts rather than the superposition of sets of unrelated astrophysical objects with distinct, less variable spectra.

Variability of the burst production mechanisms is evident in the spectral changes observed within individual bursts. Comparisons of the peak flux spectra to the total fluence spectra show that in general the peak flux is significantly harder than the total fluence in the energy range 20–100 keV. The peak flux is harder than the total fluence in the 50–300 keV and the $E > 300$ keV ranges as well, although the effect is not as significant.

REFERENCES

- Band, D. L., et al. 1993, *ApJ*, 413, 281
 Cline, T. L., Desai, U. D., Klebesadel, R. W., Strong, I. B., et al. 1973, *ApJ*, 185, L1
 Fishman, G. J., et al. 1989a, in *Proc. GRO Science Workshop*, Vol. 2, ed. N. Johnson (Washington, DC: NRL), 39
 ———. 1989b, in *Proc. GRO Science Workshop*, Vol. 3, ed. N. Johnson (Washington, DC: NRL), 47
 Harmon, B. A., et al. 1993 in *Proc. Compton Observatory Science Workshop*, ed. R. Shrader, N. Gehrels, & B. Dennis (NASA CP 3137), 69
 Higdon, J. C., & Lingelfelter, R. E. 1990, *ARA&A*, 28, 401
 Jung, G. V. 1989, *ApJ*, 338, 972
 Kouveliotou, C., Meegan, C. A., Fishman, G. J., Bhat, N. P., Briggs, M. S., Koshut, T. M., Paciesas, W. S., & Pendleton, G. N. 1993, *ApJ*, 413, L101
 Kwok, P. W., et al. 1993, in *AIP Conf. Proc. 280, Proc. Compton Gamma-Ray Observatory Conf.*, ed. M. Friedlander, N. Gehrels, & D. Macomb (New York: AIP), 885
 Matz, S. M., et al. 1985, *ApJ*, 288, L37
 Mazets, E. P., et al. 1981, *Ap&SS*, 80, No. 1, 3
 ———. 1988, *Adv. Space Res.*, Vol. 8, No. 2–3, (2) 669
 Meegan, C. A. 1991, in *BATSE Flight Software User's Manual*
 Mitrofanov, I. G., et al. 1992, in *Gamma-Ray Bursts: Observations, Analyses, and Theories*, ed. C. Ho, R. Epstein, & E. Fenimore (Cambridge Univ. Press), 209
 Murakami, T., et al. 1988 *Nature*, 335, 234
 Pendleton, G. N., Paciesas, W. S., Lestrade, J. P., Fishman, G. J., Wilson, R. B., & Meegan, C. A. 1989, in *Proc. GRO Science Workshop*, Vol. 4, ed. N. Johnson (Washington, DC: NRL), 547
 Pendleton, G. N., et al. 1992, in *Proc. Compton Observatory Science Workshop*, ed. R. Shrader, N. Gehrels, & B. Dennis (NASA CP 3137), 47
 Wheaton, W. A., et al. 1973, *ApJ*, 185, L57

Report Document Page

1. Report No.		2. Government Accession No.		3. Recipient's Catalog No.	
4. Title and Subtitle "BATSE Data Analysis" Final Report				5. Report Due June 21, 1995	
				6. Performing Organization Code University of Alabama in Huntsville	
7. Author(s) William S. Paciesas				8. Performing Organization Report No.	
				10. Work Unit No.	
9. Performing Organization Name and Address University of Alabama in Huntsville Huntsville, Alabama 35899				11. Contract or Grant No. NAS8-38609, D. O. 100	
12. Sponsoring Agency Name and Address National Aeronautics and Space Administration Washington, D.C. 20546-001 Marshall Space Flight Center, AL 35812				13. Type of report and Period covered Final February 16, 1994 - May 15, 1995	
				14. Sponsoring Agency Code	
15. Supplementary Notes					
16. Abstract Miscellaneous tasks related to the operation of, and analysis of data from, the Burst and Transient Source Experiment (BATSE) on the Compton Gamma Ray Observatory (CGRO) were performed. The results are summarized and relevant references are included. Selected scientific papers produced as a result are attached.					
17. Key Words (Suggested by Author(s)) Gamma-ray astronomy				18. Distribution Statement Unclassified-Unlimited	
19. Security Class. (of this report) Unclassified		20. Security Class. (of this page) Unclassified		21. No. of pages 40	
				22. Price	

